

Measurement of Optical Properties of Fruits and Vegetables: A Review

Renfu Lu^{1,*}, Robbe Van Beers², Wouter Saeys², Changying Li³, Haiyan Cen⁴

¹U.S. Department of Agriculture Agricultural Research Service, East Lansing, Michigan, USA

²KU Leuven, Department of Biosystems, MeBioS, Kasteelpark Arenberg 30, 3001, Leuven, Belgium

³College of Engineering, University of Georgia, Athens, Georgia, USA

⁴College of Biosystems Engineering and Food Science, Zhejiang University, Hangzhou, China

* To whom corresponding should be sent. Email: renfu.lu@usda.gov (R. Lu)

Abstract

This paper provides an overview of the principles and theory of measuring optical properties of biological materials. It then presents the instrumentation and data analysis procedures for implementing several emerging optical techniques, including spatially resolved, time-resolved, and spatial-frequency domain, along with the standard integrating sphere method. Applications of these techniques for optical property measurement, maturity and quality assessment, and defect detection of fruits and vegetables are then reviewed, followed with discussions on issues and challenges that still need to be addressed for these emerging optical techniques. While these optical techniques are overall more sophisticated in instrumentation and computation, they are based on solid radiative transfer theory or diffusion approximation theory. Hence, measurement of optical absorption and scattering properties has the potential of providing more complete, objective information for quality evaluation of horticultural products. At present, these techniques are still slow in measurement, and prone to errors due to modeling and instrumentation deficiencies. Further research is therefore needed in using a better mathematical

26 modeling approach, improving data acquisition accuracy and speed, and developing more robust
27 inverse algorithms for optical property estimations.

28

29 **Keywords:** Spatially resolved, time-resolved, spatial-frequency domain, postharvest quality,
30 fruit, vegetable.

31

32 **1. Introduction**

33 Optical imaging and spectroscopic techniques now are widely used for property, quality and
34 safety assessment of horticultural and food products. Most of these techniques rely on
35 measurement and direct analysis of the output optical signals (i.e., spectra and/or images in the
36 form of reflection or transmittance) acquired from food samples under a specific form of lighting
37 (i.e., diffuse or uniform lighting, point lighting, patterned lighting, etc.). This type of approach,
38 which may be termed the direct approach, overall is simpler, faster and easier to implement for
39 online or offline applications, compared to the optical measuring methods reviewed in this paper,
40 which belong to the inverse or indirect approach. Conventional visible and near-infrared
41 (Vis/NIR) spectroscopy employs the direct approach to measure the aggregate amount of light
42 either reflected from or transmitted through a biological or food material, resulting from the
43 combined effect of absorption and scattering of photons by the tissues. The acquired spectral
44 data are then processed, via mathematical techniques, for establishing a quantitative or
45 qualitative relationship with the property or quality parameter(s) of interest. Once the calibration
46 model is established and validated, it can then be used for predicting new samples. There are,
47 however, some inherent shortcomings with conventional Vis/NIR technique and the direct
48 approach in general, because the measured values of reflectance or transmittance are extrinsic or

49 phenomenological values (like force and pressure in mechanical measurements), and they are
50 influenced by such factors as type of instrument, sensing mode (reflectance, transmittance, etc.),
51 and light source/detecting probe setup. It thus presents great challenges in transferring the
52 Vis/NIR calibration models between different instruments or comparing the performance of
53 different instruments.

54 In recognizing the shortcomings or limitations of conventional Vis/NIR technique or the
55 direct approach in general, researchers have long sought alternative approaches to measure
56 optical absorption and scattering properties of food and biological materials. They are two
57 intrinsic material properties that characterize the behavior of light interaction with biological
58 tissues. Hence, the measured values for the two optical property parameters are, in principle,
59 independent of instrumentation type and lighting/detecting probe setup, which would make it
60 easier to compare the data acquired from different instruments for different studies. In this paper,
61 the terms ‘optical properties’ and ‘bulk optical properties’ are used interchangeably, both
62 referring to the average effect of different optical processes occurring in tissues at the
63 microscale. The light interaction with tissues can be described with two optical parameters related
64 to the two basic processes, i.e., absorption and scattering. Absorption is largely determined by
65 the chemical composition of the tissue, while scattering is dependent on density and tissue
66 structures (e.g., particle size, distributions, etc.). Hence, measurement of the two optical
67 parameters could provide more complete, objective information about the structural and
68 chemical properties of samples.

69 Early efforts had been made by Birth and colleagues in the late 1970s and early 1980s on
70 measuring the optical absorption and scattering properties of food products, based on the
71 empirical model (i.e., Kubelka-Munk model) for two-dimensional turbid slabs (Birth, 1978,

72 1982; Birth et al., 1978). However, due to the limitations of optical and computer technologies
73 available at that time, the measurement procedure, which involved both reflectance and
74 transmittance, was quite tedious and time consuming. Nevertheless, these early studies provided
75 an alternative approach for optical property measurement, and they also demonstrated some
76 merits of using optical absorption and scattering parameters for assessing properties and quality
77 attributes of food products.

78 From the late 1980s to the 2000s, rapid advances were made in Vis/NIR technique in both
79 hardware and software (i.e., chemometrics). A large variety of Vis/NIR instruments became
80 available, from expensive benchtop instruments to low-cost, miniaturized handheld devices.
81 Chemometric techniques also evolved from conventional linear modeling to nonlinear modeling
82 and to artificial neural networks. Thanks to these developments, Vis/NIR spectroscopy has
83 spread into different areas of food and agriculture applications as well as many other industries
84 (e.g., pharmaceutical and chemical), as shown by the exponential increase in scientific
85 publications over that period of time (Nicolai et al., 2007). In comparison, little progress was
86 made on optical property measurement of food and agricultural products in the 1990s, with only
87 a few, sporadic scientific publications. However, the situation was completely different in
88 biomedical optics research. Since the mid-1980s, significant advances have been made in
89 noninvasive (also called *in vivo* in the biomedical optics field) techniques for measuring optical
90 absorption and scattering properties of biological materials, thanks to major breakthroughs in
91 analytical solutions to the theory of light transfer as well as optical detection and laser
92 technologies. Specifically, analytical solutions to the diffusion approximation theory, a
93 simplification to the radiative transfer theory, became available for several special, important
94 illumination conditions (i.e., steady-state or continuous-wave point lighting, pulsed point-

95 lighting and frequency modulated lighting) (Farrell et al., 1992; Kienle and Patterson, 1997;
96 Patterson et al., 1989, 1991). Based on these analytical models, several new techniques,
97 including spatially resolved (SR), time-resolved (TR) and frequency-domain (FD), were
98 developed for measuring optical properties of biological materials during the 1990s and 2000s
99 (Tuchin, 2007).

100 The interest in these emerging optical property measurement techniques for food and
101 agricultural products began to grow from the early 2000s, owing to the availability of more
102 affordable optical instrumentation. TR technique was first applied to measure the optical
103 properties of apples and other fruits (Cubeddu et al., 2001a, 2001b). Subsequently, a series of
104 studies were reported by a group of researchers in Italy (Rizzolo and Vanoli, 2016) on using
105 different TR instrumentation configurations (i.e., single wavelength, multi-wavelength and broad
106 spectral region) to assess quality, maturity and internal defects of fruits and vegetables. Around
107 that time period, several research groups in the U.S. and Europe also started to actively pursue
108 SR techniques for measuring optical properties of fruits, vegetables and other food products.
109 Researchers with the U.S. Department of Agriculture Agricultural Research Service
110 (USDA/ARS) at Michigan State University in Michigan, USA developed a hyperspectral
111 imaging-based SR technique for fast measurement of optical absorption and scattering properties
112 of horticultural and food products over a broad range of wavelengths (Cen and Lu, 2010; Qin
113 and Lu, 2007, 2008). Researchers at the University of Missouri, Columbia, Missouri, USA
114 developed a SR technique, based on single-fiber spectroscopy, for measuring optical properties
115 of meat muscles and meat analogs (Xia et al., 2007, 2008). Researchers from KU Leuven in
116 Belgium, used the integrating sphere method (IS), coupled with an inverse adding-doubling
117 (IAD) algorithm (hereinafter called IS-IAD), to measure the optical properties of apple, potato,

118 and meat tissue components (López-Maestresalas et al., 2015; Saeys et al., 2008; Van Beers et
119 al., 2017b; Zamora-Rojas et al., 2013). Later, the group also developed other SR sensing
120 systems, based on single-fiber, multi-fiber and imaging-based configurations, for measuring
121 fruits and food products (Aernouts et al., 2015; Nguyen Do Trong et al., 2014a, 2014b; Van
122 Beers et al., 2015). More recently, researchers from the University of Georgia at Athens,
123 Georgia, USA used IS-IAD to measure optical properties of onions and other horticultural
124 products (Wang and Li, 2013, 2014; Zhang et al., 2019).

125 In recent years, new optical property measurement techniques have continued to emerge in
126 the biomedical optics field. Researchers from the University of California at Irvine, USA
127 reported on a new spatial-frequency domain (SFD) technique for wide-area imaging of the
128 optical properties of biological tissues (Cuccia et al., 2005). The SFD technique was used to
129 detect healthy and bruised apple tissues (Anderson et al., 2007). Recently, researchers at
130 Zhejiang University, Hangzhou, China and the USDA/ARS laboratory in Michigan, USA, used
131 SFD technique to measure optical properties of fruits and food products composed of one or two
132 homogeneous layers (Hu et al., 2016, 2018).

133 This paper is therefore intended to give an overview of the principles, theory and modeling of
134 light transfer in biological materials, followed by a brief introduction to the instrumentation and
135 data analysis approaches for IS-IAD, SR, SFD, and TR techniques. Applications of these
136 techniques for quality assessment of fruits and vegetables are then reviewed. Finally, discussions
137 are given on critical issues, challenges and future research needs for these techniques. This
138 review is aimed to help researchers and practitioners gain a better understanding of these
139 emerging optical property measurement techniques and their advantages and limitations, thus
140 stimulating further research in optical property measurement of horticultural and food products.

141 2. Principles and Theory of Light Transfer

142 2.1 Light transfer in biological materials

143 Biological or plant tissues are a complex system formed by cells and their extracellular
144 matrix. These cells and extracellular matrix contain different components like membranes,
145 cytoskeletons, organelles, etc., each of which has different structural, chemical and optical
146 characteristics. Hence, the actual process of light interaction with the biological tissue system is
147 rather complex at the microscale. However, in studying light transfer in biological or plant
148 tissues, they may be treated as being primarily composed of scattering (e.g., the organelles and
149 cellular membranes) and absorbing (e.g., chromophores) particles. Under this simplified
150 treatment, light transfer in biological tissues mainly involves the process of photon interactions
151 with the scattering and absorbing particles. As photons enter the plant tissues, they will move
152 straightforward until encountering a scattering or absorbing particle. The photons will change the
153 travelling direction (called scattering) upon hitting the scattering particle, or they would be
154 absorbed, if the particle is an absorbing particle and when the level of energy for the photons
155 matches that of the particle according to quantum theory. The actual change in the scattering
156 direction of the photons depends on the optical properties of the scattering particle. After the
157 particle is hit by a large quantity of photons, the angular scattering profile can be described by
158 the scattering phase function [designated as $p(\theta)$], which is unique for each particle and is
159 determined by the size, shape and orientation of the particle. Specifically, the fraction of photons
160 that would be scattered to a specific direction is determined by the anisotropy factor, designated
161 as g . Values of g range between -1 and 1, where $g=-1$ is total backward scattering; $g=0$ is
162 isotropic scattering (i.e., photons scatter equally in all directions), and $g=1$ represents total
163 forward scattering. For most food and plant materials, g values range between 0.7 and 0.9,

164 indicating that forward scattering is dominant. The absorption process can be characterized by
 165 the absorption coefficient, normally designated as μ_a . On the other hand, the scattering process is
 166 defined by the scattering coefficient (μ_s) and the anisotropy factor (g). Hence, with the
 167 knowledge of μ_a , μ_s and g , one can, in principle, describe the transfer of photons in biological
 168 tissues. As shown in the following section, when scattering is dominant (i.e., $\mu_s \gg \mu_a$), the
 169 anisotropy factor can be lumped into the scattering coefficient, which leads to a new optical
 170 parameter, called the reduced scattering coefficient [i.e., $\mu_s' \equiv (1-g)\mu_s$]. This means that for most
 171 plant materials like fruits and vegetables, it would be sufficient to use μ_a and μ_s' for
 172 characterizing the interaction of light with the plant material.

173 2.2 Diffusion approximation theory

174 The transfer of light in biological materials is best described by radiative transfer theory. The
 175 radiative transfer equation can be derived by employing the principle of conservation of energy.
 176 A detailed description on the derivation of the radiative transfer equation can be found in Lu
 177 (2016). Since the radiative transfer equation is expressed in an integro-differential form with six
 178 variables, it cannot be solved analytically, except for a few special, restricted situations.
 179 Subsequently, the assumption of dominant scattering in turbid biological materials is used to
 180 approximate it as by a diffusion equation:

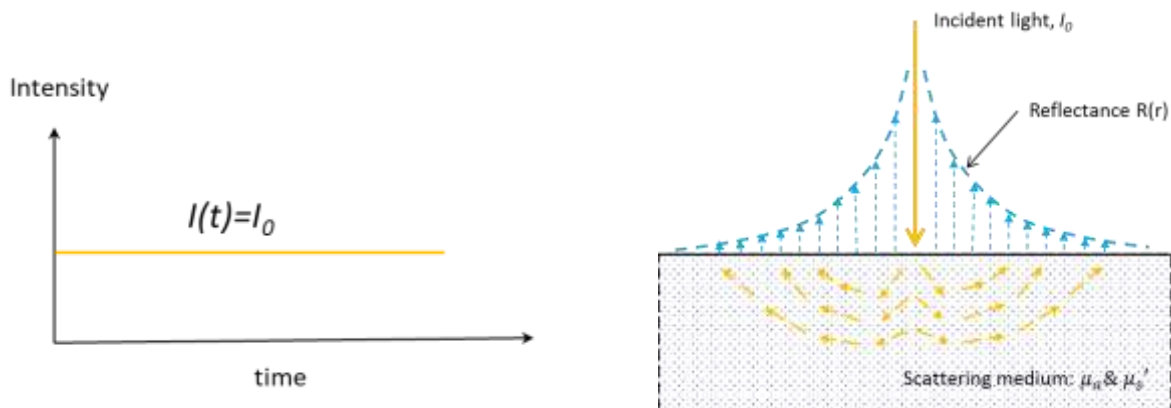
$$181 \quad \frac{\partial \Phi(\vec{r}, t)}{\partial t} = \nabla \cdot [D \nabla \Phi(\vec{r}, t)] - \mu_a \Phi(\vec{r}, t) + S(\vec{r}, t) \quad (1)$$

182 where $\Phi(\vec{r}, t)$ is the fluence rate, \vec{r} is the location vector, t is the time variable, $S(\vec{r}, t)$ is the
 183 isotropic source in the medium, and D is called the diffusion coefficient, which is given by

$$184 \quad D = \frac{1}{3[\mu_a + (1-g)\mu_s]} = \frac{1}{3(\mu_a + \mu_s')} \quad (2)$$

185 where μ_s' is the reduced scattering coefficient. The diffusion equation only contains two

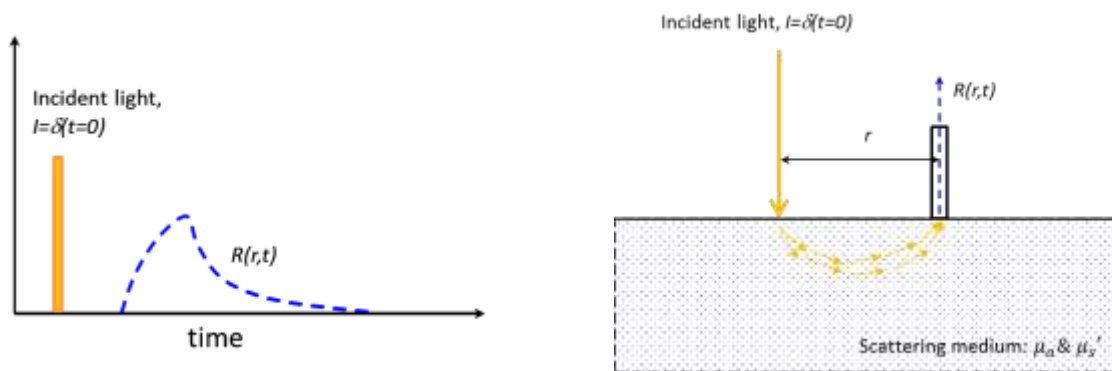
186 independent optical parameters, i.e., the absorption and reduced scattering coefficients, and it has
 187 been solved analytically for several special, important illumination situations, as shown in Figure
 188 1, which include continuous-wave or steady-state point lighting (Figure 1a), pulsed point lighting
 189 (Figure 1b), frequency-modulated point lighting (Figure 1c), and spatially-modulated area
 190 lighting (Figure 1d) (Lu, 2016). These analytical solutions form the theoretical basis for the SR,
 191 TS, FD, and SFD techniques described in Section 3.



192

193

(a)

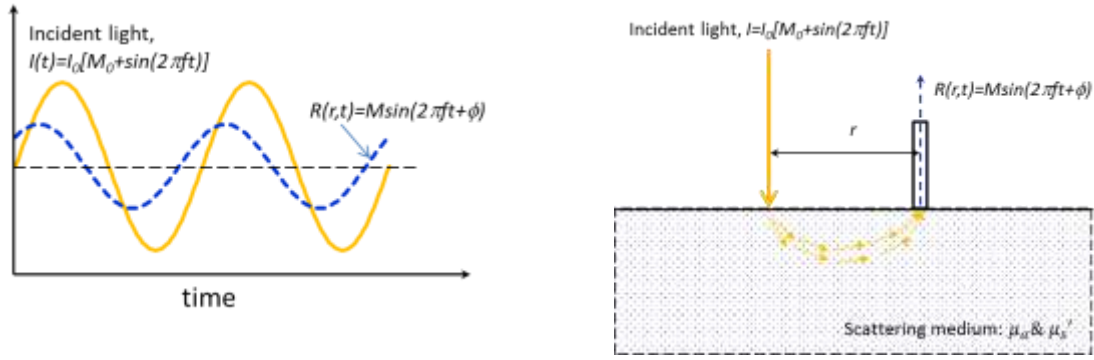


194

195

(b)

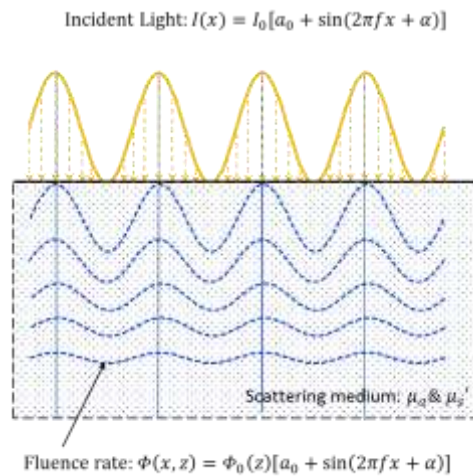
196



197

198

(c)



199

200

(d)

201 Figure 1. Four special cases of light illumination at the surface of a semi-infinite turbid medium,
 202 for which analytical solutions to the diffusion approximation equation are available: a)
 203 continuous-wave point lighting (time-independent), b) short-pulsed lighting, c) frequency-
 204 modulated point lighting, and d) spatially-modulated area lighting (time-independent), where
 205 symbol I represents the intensity of the incident light, f is the frequency either in the time (t) or
 206 spatial domain. It should be noted that in cases a) through c), the spatial dimensions are
 207 expressed in the two-dimensional polar coordinate system, while in case d), they are in the two-
 208 dimensional Cartesian coordinate system.

209

210 2.3 Numerical simulations

211 Although the diffusion equation is widely used with SR, SFD and TR/FD techniques for
212 estimating optical properties of biological materials, it is only applicable when scattering is
213 dominant over absorption ($\mu_s \gg \mu_a$) and if the radiance is only considered at a sufficiently large
214 distance from the point of illumination (\gg one mean free path) (Martelli et al., 2010). In the
215 Vis/NIR region of the spectrum, these assumptions do not always hold for biological tissues, due
216 to the high absorption by biological chromophores, of which chlorophyll, carotenoids,
217 anthocyanins and water are dominant in plant materials. To overcome these limitation
218 researchers have used numerical methods, such as adding-doubling (AD) and Monte Carlo (MC)
219 methods, to simulate light propagation in biological tissues (Prahl et al., 1993; Simpson et al.,
220 2001; Tuchin, 2017; Wang et al., 1995).

221 The AD method, which was first introduced by van de Hulst (1980), is used to numerically
222 solve the radiative transfer theory (RTT) for an infinitely thin and single-scattering homogeneous
223 layer by calculating the angle-dependent reflection and transmission of that layer (Prahl, et al.,
224 1993). With the assumption of single scattering, the RTT can be solved with relative ease for a
225 series of bulk optical properties (BOP) (i.e., μ_a , μ_s , and $p(\theta)$). By adding layers with different
226 optical properties, dissimilar slabs with internal reflections at the boundaries can be accounted
227 for. Likewise, the differences in refractive indices n between two materials, causing refraction
228 and reflection at the boundaries, can be accounted for, respectively, using Snell's and Fresnel's
229 laws. Eventually, for a specific sample slab, the AD routine results in angular reflectance and
230 transmittance functions per wavelength. Integrating these functions over the different conical
231 segments provides the total reflectance and total transmittance of the sample slab. The equations
232 and algorithm of the AD method have been described in Prahl (1995). The AD approach is fast

233 and accurate, but it is restricted to layered geometries and cannot be used to retrieve information
234 on the spatial distribution of the reflected and transmitted photons (Aernouts et al., 2014).
235 Moreover, each layer should have homogeneous BOP. The routine has been extended to estimate
236 the spectral and angular distribution of the scattered radiation of (fluorescent) materials (Leyre et
237 al., 2012), while it can also be inverted to retrieve the BOP for thin sample slabs from the
238 measured total transmittance and total reflectance, as described in Section 3.1 (Aernouts et al.,
239 2013; Prahl et al., 1993).

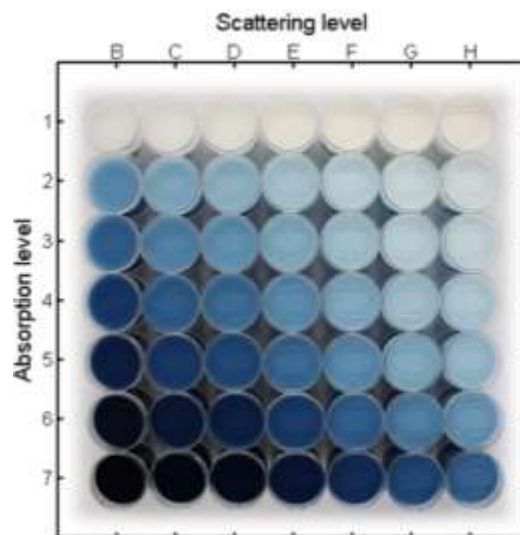
240 MC simulation is widely used for modeling light propagation in turbid biological tissues,
241 owing to its flexibility and simplicity in simulating the energy transfer process in arbitrary
242 geometries with complex boundary conditions or spatial localization of inhomogeneities. MC
243 methods provide a probabilistic approach to simulate the random walk of photons in absorbing
244 and scattering media (Watté et al., 2016). Photons are traced through a turbid medium until they
245 exit at the sample surface or until they are absorbed. Photon movement from one photon-tissue
246 interaction to the next is described by probability functions using the tissue's optical properties.
247 Repeating this process for a large number of photons results in an estimation of photon
248 distributions in the tissue (Wang and Jacques, 2000). Classic MC algorithms, such as the MC
249 code for multi-layered media, allow to simulate light propagation in multi-layered, semi-infinite
250 slabs (Wang et al., 1995). Moreover, the MC method can also be used in a structured finite mesh
251 approach, in which photons move in a tetrahedral mesh (Watté et al., 2015a). This approach
252 allows to describe more complex biological structures, including targets with curved boundaries
253 or locally refined structures, like tissue cells and intercellular spaces. Finally, meshless
254 approaches can be studied using particle-based simulations, in which photons and scattering
255 particles are defined as particles, while the interaction of light with spherical scattering particles

256 can be determined using the exact Mie solution. However, because of the large number of
257 photons (typically 10^4 to 10^6) that need to be simulated to reduce the effects of stochastic noise,
258 MC simulations are generally computationally intensive (Tuchin, 2007).

259 To overcome some shortcomings of the previously described MC techniques (e.g., long
260 computational time and oversimplifications in describing the photon-particle interactions) and to
261 better deal with noise, which is inherently present when modelling data retrieved from optical
262 measurements, stochastic data-based surrogate models, often referred to as ‘metamodels’, have
263 been introduced as a computationally cost-effective alternative for solving the RTT for light
264 propagation (Aernouts et al., 2015; Watté et al., 2013). These metamodels directly establish the
265 link between the design space (input parameters) and the performance space (output parameters)
266 (Simpson et al., 2001). These models would be trained by using the data obtained from MC
267 simulations or optical measurements on samples with known BOP. Building a metamodel based
268 on MC simulations would provide high flexibility. However, the estimation procedure can be
269 simplified by linking optical measurements on known samples directly with the BOP. This has
270 the advantage that in future predictions, using the same optical measurement technique, both
271 light propagation characteristics and measurement geometry used are accounted for (Watté et al.,
272 2013). To achieve this goal, so-called optical phantoms, designed with known optical properties,
273 are measured with the same optical setup as that used for the actual measurements on the desired
274 products. By doing this, a possible mismatch between simulation and measurement setup can be
275 avoided. To use these phantom measurements for building a metamodel, a set of phantoms
276 describing a wide range of absorption and scattering properties should be designed so that they
277 are representative for the BOP of the measured products. Three different key components should
278 be considered when designing optical phantoms: (1) the matrix material, (2) the type of absorber

279 and (3) the scattering agent (Pogue and Patterson, 2006). The phantom ingredients should be
280 chosen carefully to avoid interactions between the components, as these might affect the
281 estimation of the BOP.

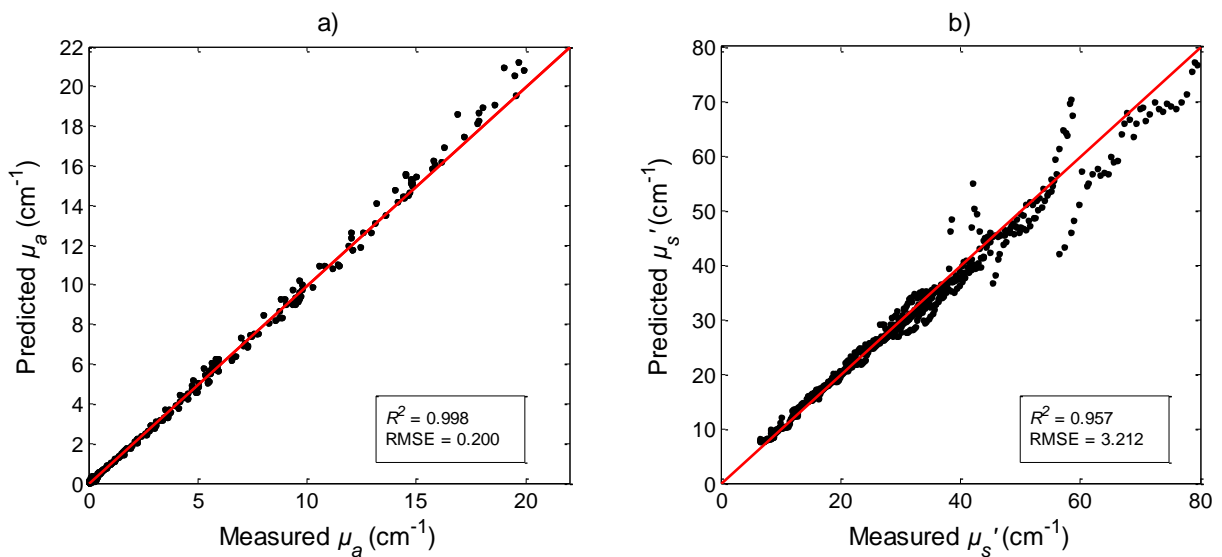
282 An example of creating a set of liquid optical phantoms by combining Naphthol Blue Black
283 (NBB) as an absorber (peak absorption at 618 nm) and Intralipid[®] 20% as a scattering agent, is
284 shown in Figure 2. The rows (from number 1 to 7) have an increasing level of absorption, while
285 the columns (from letter B to H) have an increasing level of scattering. The reference BOP
286 values, measured using a double integrating sphere (DIS) setup (Aernouts et al., 2013), served as
287 an input for building a forward metamodel, linking bulk optical properties to the diffuse
288 reflectance values at different distances from the point of illumination. The diffuse reflectance
289 was measured using a contactless hyperspectral scatter imaging setup.



290 3

291 Figure 2. Set of 49 calibration phantoms made by combining Intralipid[®] 20% (IL) as a
292 scattering agent, Naphthol Blue Black (NBB) as an absorber and water as a dilution agent.
293 The concentration of IL increases from left to right (level B to H), while the concentration
294 of NBB increases from top to bottom (level 1 to 7).

295 A metamodel combining 30 source-detector distances was evaluated using a set of validation
 296 phantoms. The performance of the metamodel for the BOP estimations of 8 validation phantoms
 297 at 91 different wavelengths (from 550 nm to 1000 nm in steps of 5 nm) is illustrated in Figure 3.
 298 The bulk absorption coefficient was predicted with an R^2 of 0.998 and a root mean squared error
 299 for validation (RMSE) of 0.200 cm^{-1} (Figure 3a), which are in agreement with the results
 300 reported by Watté et al. (2015b), when a translation-stage SR setup was employed. Predicted
 301 values for μ_s' , especially above 40 cm^{-1} , are less accurate, with an R^2 of 0.957 and an RMSE of
 302 3.212 cm^{-1} . This could have possibly been caused by the design of the set of calibration
 303 phantoms, as values close to the edges of this design showed larger prediction errors.



305 Figure 3. Scatter plots of predicted versus measured (a) bulk absorption coefficient μ_a and
 306 (b) reduced scattering coefficient μ_s' for the validation phantoms. The red lines indicate the
 307 1:1 line.

308 Finally, Aernouts et al. (2014) proposed and validated a flexible tool for simulating the BOP
 309 of polydisperse spherical particles in an absorbing host. A microscale model was used as the base

310 for a multiscale model predicting the BOP of polydisperse systems. By using the Mie solution
311 for Maxwell's equations, the optical properties of a spherical particle in an absorbing host were
312 simulated. Polydispersity of the particle systems was then supported by discretization of the
313 provided particle size distributions. The number of intervals was optimized automatically in an
314 iterative procedure. As a result, the BOP of the polydisperse system could be obtained in a
315 flexible way. Two aqueous nanoparticle systems and an oil-in-water emulsion (Intralipid® 20%)
316 were used for validating the developed tool. The simulated BOP values were compared to the
317 reference BOP measured using a DIS and unscattered transmittance setup (described in Section
318 3.1). This study showed that this type of simulation based on the particle size distribution of the
319 scattering particles matched closely ($R^2 \geq 0.899$) with the BOP values obtained by the reference
320 measurements. Postelmans et al. (2018) implemented this microscale light propagation tool in an
321 inverse estimation algorithm to develop a shape dependent method for the estimation of particle
322 size distributions from bulk scattering coefficient spectra. They successfully validated this
323 method on simulated data for polystyrene in water suspensions and investigated its sensitivity to
324 measurement errors. They found that a correct estimate for the refractive index mismatch
325 between the particle and the medium is most critical.

326

327 **3. Measurement Techniques**

328 In this section, we first describe the integrating sphere technique (i.e., IS-IAD), which is
329 often used as a reference method for evaluating other new techniques, and then the three
330 nondestructive measurement techniques (i.e., SR, TR, and SFD), based on the light illumination
331 conditions presented in Figure 1. All the techniques have been used for measuring optical
332 properties of fruits and vegetables.

333 3.1. Integrating sphere

334 3.1.1 Instrumentation

335 Integrating spheres have been commonly used as an optical calibration and measurement tool
336 and in particular they have been successfully used to measure optical properties of tissues
337 (Jacquez and Kuppenheim, 1955; Tuchin, 2007). The inner surface of an integrating sphere is
338 uniformly coated with highly reflective diffuse materials (e.g., reflectivity $\rho = 0.98$) to achieve
339 homogenous distributions of light radiation at the sphere's inner wall. A light beam falling on the
340 inner surface of an integrating sphere is evenly scattered to all directions (i.e., Lambertian
341 reflections) and the light fluxes are evenly distributed (spatially integrated) on the homogenous
342 inner surface of the sphere after multiple Lambertian reflections. A standard integrating sphere
343 usually has three ports: input port, exit port, and a third port for detector. Plugs with highly
344 reflective materials are also needed to cover the port that should be closed. For real integrating
345 spheres, the surfaces do not have perfect Lambertian reflection. To prevent measurement errors
346 by specular reflection, baffle(s) coated with a highly reflective material is often placed inside the
347 sphere to further diffuse the specular reflection and avoid the direct reflection from reaching the
348 detector. In certain applications, the fourth port is also used so that the specular reflection beam
349 can go out from the sphere in a light trap.

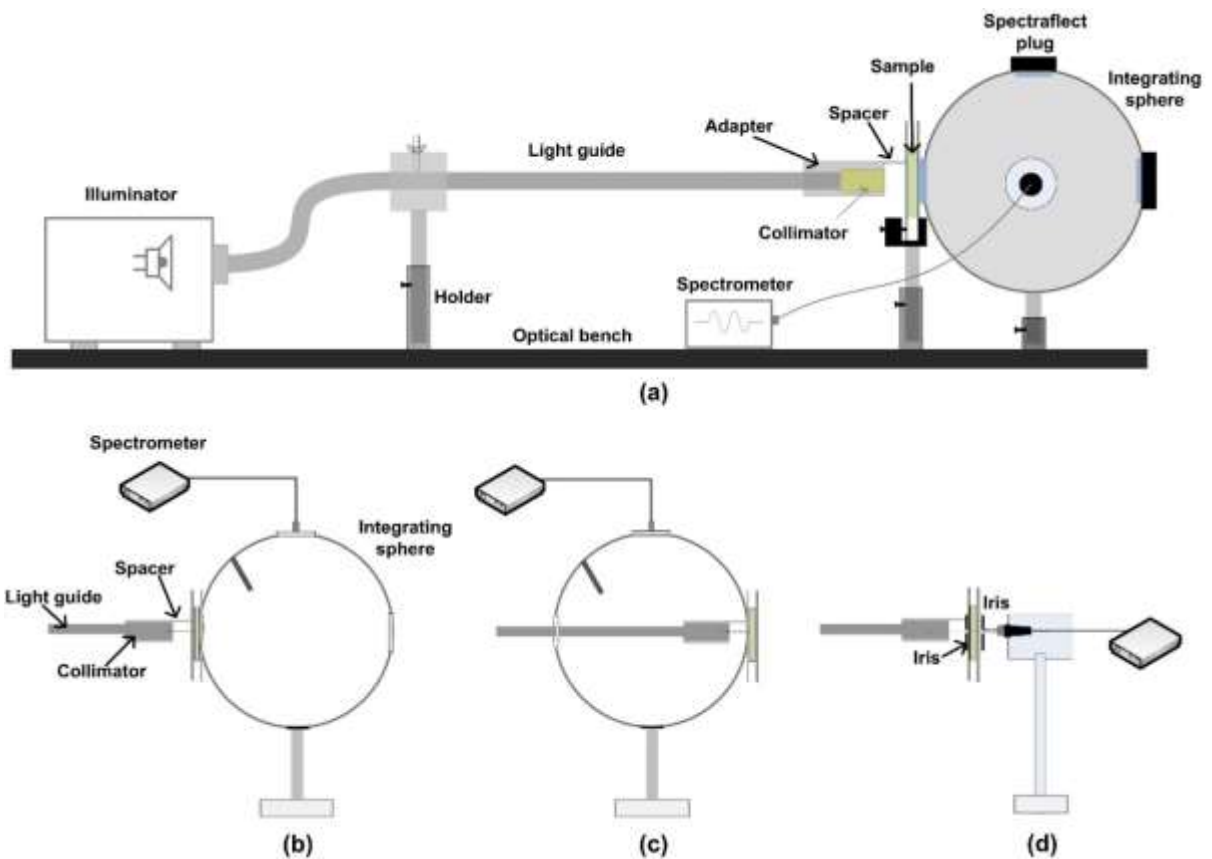
350 There are several advantages of using integrating sphere techniques to measure the spectral
351 reflectance and transmittance of fruit and vegetable tissue samples, in comparison to directly
352 measuring the sample by a spectrometer. First, in a regular spectrometer measurement where the
353 incident light directly impinges on the sample surface, the detected reflectance often has a
354 dependency on the angle and distance between the incident beam and the detector. When an

355 integrating sphere is used, the fluxes reflected on the sample are all captured and normalized by
356 the sphere. Thus, the angular dependency is no longer an issue. Second, the detector-object
357 distance is often fixed in the integrating sphere measurement. Even if there is a small change
358 between the sample-sphere distance, it will not affect the results of the measurements as long as
359 all reflected light bounces back into the sphere. Additionally, by using integrating spheres, the
360 spectral measurements are less dependent on the shape of the light beam and the homogeneity of
361 the sample, since both incident light beam and the reflected/scattered light will be normalized on
362 the inner surface of the sphere before being captured by the detector.

363 Figure 4a shows an example of the instrumentation setup of an integrating sphere system for
364 collecting the spectra of vegetable tissues (Wang and Li, 2014). The system consisted of an
365 integrating sphere, a spectrometer, a light source, optical fibers, a collimator, and a slab of tissue
366 sample sandwiched between glass slides. The integrating sphere (model 4P-GPS-060-SF,
367 Labsphere, Inc., North Sutton, NH, USA) had an internal diameter of 152 mm and four 25.4 mm
368 diameter ports at 0° , 90° , 180° , and the north pole. The sphere was coated with a highly reflective
369 material (Spectrafect[®], Labsphere, Inc., North Sutton, NH, USA), whose reflectivity was greater
370 than 98% in the test spectral range. A Vis/NIR spectrometer (model USB4000, Ocean Optics,
371 Dunedin, FL, USA) and a NIR spectrometer (model CD024252, Control Development, Inc.,
372 South Bend, IN, USA) were used to measure light signals for the two spectral ranges of 550 –
373 880 nm and 950 – 1650 nm, respectively. An optical fiber (400 μm diameter and 0.37 numerical
374 aperture) (model M32L02, Thorlabs, Newton, NJ, USA) was used to deliver the light to the
375 spectrometer from the integrating sphere. The light source was provided by a DC-regulated fiber
376 optic illuminator (model DC-950, Dolan-Jenner Industries, Boxborough, MA, USA) with a
377 goose neck light guide. The collimator mounted in front of the light guide was used to collimate

378 the divergent light of the fiber optic illuminator to a 1.5 mm diameter light beam. Each vegetable
379 tissue sample was sandwiched between two pieces of Borofloat glass slide (transmittance >
380 90%), covering the whole entrance or exit port of the integrating sphere.

381 The total transmittance T was measured when the sample was placed in front of the entrance
382 port of the sphere and the opposite exit port was covered by a Spectrafect plug (Figure 4b). The
383 total reflectance R was measured when the sample was placed behind the exit port (Figure 4c).
384 To measure collimated transmittance T_c , a 1-mm diameter iris was placed between the collimator
385 and the sample to constrain the position and the size of the incident beam, and the other iris in
386 front of the detector blocked the ambient scattered light from entering the spectrometer (Figure
387 4d) (Prahl, 2011).

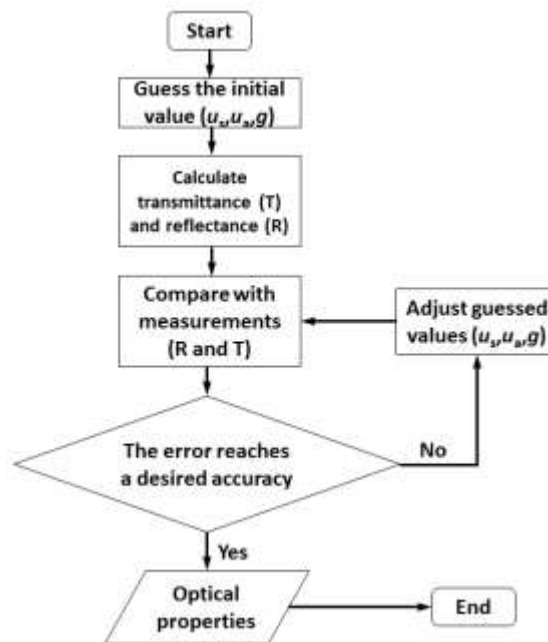


388

389 Figure 4. The hardware components of the integrating sphere-based spectroscopic system (a),
390 and the schematics for measuring the three types of spectra: the total transmittance T (b), the
391 total reflectance R (c), and the collimated transmittance T_c (d) (Wang and Li, 2014).

392 3.1.2 Data analysis

393 The optical responses (R , T , and T_c) measured using the spectrometer and the integrating
394 sphere are processed by the inverse adding-doubling (IAD) algorithm to obtain the optical
395 properties of fruit and vegetable tissue samples. IAD (Pickering et al. 1993; Prahl et al., 1993) is
396 one of the most common and accurate methods to calculate the light scattering and absorption
397 coefficients of samples based on their reflectance and transmittance (Tuchin, 2007). It is the
398 inverse algorithm of the adding-doubling method, which has been described in Section 2.3. The
399 general procedure of the IAD algorithm is illustrated in Figure 5.



400

401 Figure 5. Flowchart of the inverse adding-doubling (IAD) algorithm.

402

403 In implementing the IAD method, it is essential to measure the reflectance and transmittance
404 of the sample by integrating spheres. In addition to the method introduced in the previous section
405 using a single integrating sphere to measure reflectance and transmittance, double integrating
406 sphere setups can also be used to obtain both reflectance and transmittance measurements
407 simultaneously (Pickering et al., 1993, Aernouts et al., 2013). The double integrating sphere
408 setup with single beam is simple to construct and use, but it requires two integrating spheres.

409 In the past decade, the IS-IAD method has been used to measure the optical properties of
410 food items. For instance, Saeys et al. (2008) and Van Beers et al. (2017b) measured the μ_a , μ_s
411 and g of the apple skin and flesh in 350-2200 nm using a double integrating sphere configuration
412 in combination with the IAD method for different apple cultivars and at different maturation
413 stages. Lopez-Maestresalas et al. (2015) measured the optical properties of potato flesh in the
414 500-1900 nm range. Wang and Li (2013) measured the optical properties of the skin and flesh of
415 four common types of onions at 633 nm and reported that the optical properties of onion tissues
416 were significantly different between onion cultivars. The group also used the IS-IAD method to
417 investigate the optical properties of healthy and diseased onion tissues in a broad spectrum (550-
418 880 nm and 950-1650 nm) (Wang et al., 2014). Fang et al. (2016) used a similar method to
419 measure absorption and scattering coefficients of kiwifruit tissues at the wavelength of 633 nm.
420 The IS-IAD method also provides good reference measurements for the development of other
421 techniques (e.g., SR, TR and MC) for measuring optical properties of food items (Cen et al.,
422 2013; Lu, 2008; Qin and Lu, 2009).

423 3.2 Spatially resolved

424 Spatially resolved (SR) technique was first developed by Reynolds et al. (1976) for
425 understanding light propagation in turbid media. Later, Langerholc (1982) and Marquet et al.
426 (1995) reported that SR measurements can be used to determine optical properties of biological
427 tissues. In this method, a small continuous-wave light beam perpendicularly illuminates the
428 sample's surface, and the reemitted light is measured at different distances from the light source
429 (Figure 1a). The absorption coefficient (μ_a) and the reduced scattering coefficient (μ_s') can then
430 be extracted from the measured SR reflectance profiles by using a numerical method or an
431 appropriate analytical solution to the diffusion equation, coupled with an inverse algorithm.

432 3.2.1 Instrumentation

433 SR technique is well suited for use in postharvest applications thanks to its low
434 instrumentation cost, easy implementation and nondestructive measurement setup. Hence, many
435 different SR measurement configurations have been developed for horticultural and food
436 products. Optical fiber arrays and non-contact reflectance imagery are two typical sensing
437 configurations in SR measurement (Doornbos et al., 1999; Fabbri et al., 2003; Malsan et al.,
438 2014; Pilz et al., 2008), which can be implemented with fiber optic probe (FOP), monochromatic
439 imaging (MCI), and hyperspectral imaging (HSI). Figure 6 shows four instrumental setups with
440 SR technique for measuring optical properties of fruits and vegetables. In the FOP measurement,
441 a single spectrometer, multiple spectrometers, or a spectrograph-camera combination coupled
442 with multiple detection fibers can be used to measure diffuse reflectance at different distances
443 from the light incident point (Nguyen Do Trong et al., 2014a). Figure 6a shows one of the FOP
444 configurations used for measuring optical properties of fruit and food products, which consists of
445 five optical fibers arranged at different distances. The rigid FOP only covers the maximum

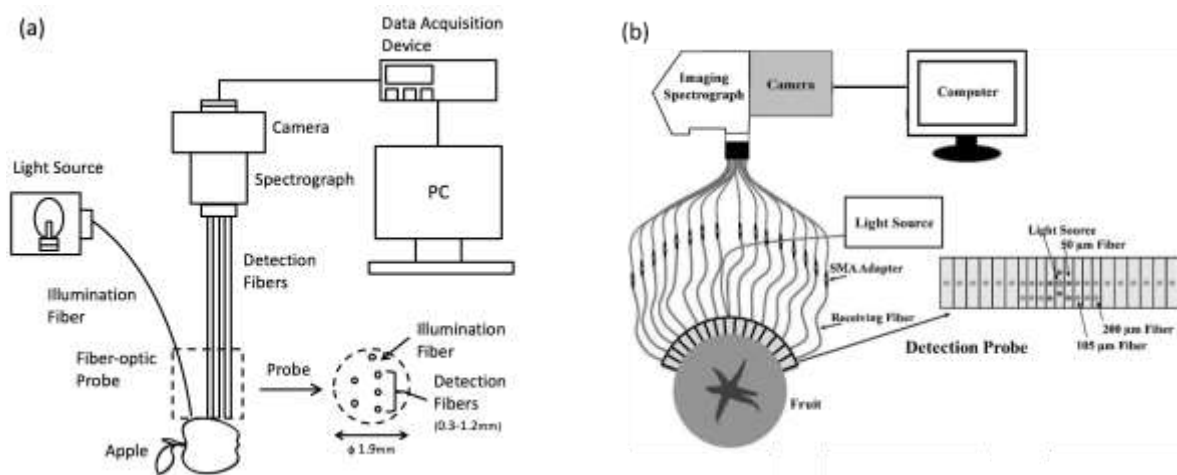
446 spatial distance of 1.5 mm and hence it can only measure tissues of homogeneous properties or
447 the superficial layer of the sample. Since most fruit and vegetable products are of curved or
448 irregular shape, a rigid FOP would have problem maintaining good contact with the sample
449 during measurement. Moreover, it is also desired or needed to measure the sample tissue at
450 greater depth. To overcome the shortcomings of a rigid FOP, a flexible FOP with 30 optical
451 fibers covering a spatial distance range of 0-30 mm was developed for measuring the optical
452 properties of fruits and vegetables (Huang et al., 2017). The optical fibers are coupled to a
453 multichannel hyperspectral imaging system, which allows simultaneous acquisition of 30 SR
454 spectra from the sample. The use of three different sizes of fibers (50, 120 and 200 μm) for the
455 probe also effectively expands the dynamic range of the camera, allowing to acquire spectra
456 from the sample at greater distances.

457 As a non-contact method, MCI is more suitable for measuring optical properties of fruits and
458 vegetables at one single wavelength. A laser diode or a combination of a supercontinuum laser
459 and monochromator can be used to illuminate the sample at a specific wavelength (Baranyai and
460 Zude, 2009; Van Beers et al., 2015). SR diffuse reflectance is then acquired with a CCD camera
461 (Figure 6c). This SR configuration is simple and relatively easy to implement. The acquired 2-D
462 scattering images are reduced to 1-D scattering profiles by radial averaging (assuming the
463 scattering images are axisymmetric with respect to the laser incident point). However, this
464 assumption does not hold for anisotropic tissues where the light is guided by the tissue fibers.
465 For example, in the case of bovine muscle tissue, the effect of the fibers resulted in scatter spots
466 with a rhombus shape (Van Beers et al., 2017a). Measurement at multiple wavelengths requires
467 sequential wavelength scanning. In addition, a substantial portion of the signal of each pixel
468 comes from the surrounding areas, which can affect measurement accuracy. Characterization of

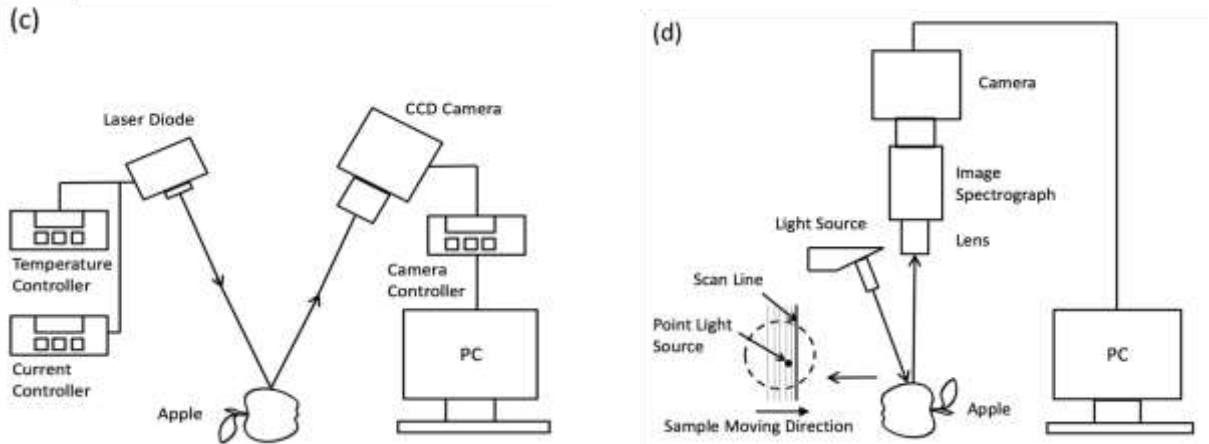
469 the point-spread function (PSF) could be helpful to obtain accurate intensity values for the image
470 data interpretation (Du and Voss, 2004; Pilz et al., 2008).

471 In hyperspectral imaging, spectral and spatial information is acquired simultaneously. This is
472 therefore advantageous for measuring SR diffuse reflectance profiles over a broad spectral range
473 (e.g., 400-1000 nm). Figure 6d shows a hyperspectral imaging-based SR system in line scan
474 mode, which mainly consists of a high-performance CCD camera, an imaging spectrograph, a
475 zoom or prime lens, a light source, and an optical fiber coupled with a focusing lens for
476 delivering a small broadband beam to the sample (Cen et al., 2012b). This SR configuration
477 allows fast acquisition of SR spectra from the sample at high spatial resolution, and it typically
478 covers a spatial distance range of about 10 mm for plant products like apples and peaches. In the
479 HSI configuration, two key factors, i.e., light beam and source-detector distance, need be
480 carefully considered in order to meet the requirements of the diffusion approximation theory
481 (Cen and Lu, 2010).

482



483



484

485 Figure 6. Schematic illustrations of (a) a fiber-optic probe with a rigid plate (Nguyen Do Trong
 486 et al., 2014a), (b) a fiber-optic probe with a flexible plate mounted with 30 optical fibers (Huang
 487 et al., 2017), (c) monochromatic imaging (Baranyai and Zude, 2009), and (d) hyperspectral
 488 imaging-based spatially resolved systems (Cen et al., 2012b).

489

490 Various studies have been reported on using different configurations of SR technique for
 491 measuring fruit and vegetables. FOP has been used for estimating optical properties of dried
 492 apples (Nguyen Do Trong et al., 2014b), fresh apples (Nguyen Do Trong et al., 2014a), and
 493 tomatoes (Huang et al., 2018). MCI technique was used for optical characterization of apples,
 494 kiwifruit, pears and oranges (Adebayo et al., 2017; Baranyai and Zude, 2009; Lorente et al.,
 495 2013; Mollazade and Arefi, 2017), while the HSI-based SR technique has been used for
 496 measuring apples, peaches, pickling cucumbers, tomatoes, and sugar beets as well as for
 497 evaluating their quality attributes (Cen et al., 2012a, 2012b; Qin et al., 2009; Van Beers et al.,
 498 2015; Zhu et al., 2015).

499

500 3.2.2 Data analysis

501 As an indirect method for optical property measurement, computation of the optical
502 parameters from the SR measurements usually requires sophisticated modeling based on the
503 radiative transfer theory, diffusion approximation, or MC simulation, coupled with appropriate
504 inverse algorithms. Numerical methods are generally required for solving the radiative transfer
505 equation or using inverse MC simulation. These methods need no or fewer physical
506 approximations on photon transport in the media, but they could be subjected to statistical
507 uncertainties during the estimation of the reflectance. One major drawback with the numerical
508 methods is that they require substantial computational time. Therefore, it has been proposed to
509 build a library of MC simulated SR profiles for a grid of μ_s , μ_a and g values. This library can
510 then be used either as a look-up table (Hjalmarsson and Thennadil, 2007; Sharma et al., 2014) or
511 for training a neural network (Hjalmarsson and Thennadil, 2008). As discussed earlier, databased
512 models, such as metamodels, can also be used to model the relation between diffuse reflectance
513 and BOP (Watté et al., 2015). This has been demonstrated both for FOP-based SR (Watté et al.,
514 2015) and HSI-based SR (Aernouts et al., 2015) systems. A popular and faster approach is to use
515 the analytical equation derived by Farrell et al. (1992) or Kienle and Patterson (1997), coupled
516 with an appropriate inverse algorithm, to obtain the estimates of μ_a and μ_s' from the acquired SR
517 diffuse reflectance profiles (Cen et al., 2012a, 2012b; Erkinbaev et al., 2014).

518 Accurate estimation of the optical parameters by inverse algorithms is not an easy task due to
519 the complexity of the analytical solutions and potential experimental errors in measuring diffuse
520 reflectance from the medium. In general, optical parameter estimation can be defined as a
521 nonlinear least squares optimization problem with several important assumptions (i.e., constant
522 variance errors, uncorrelated errors, and the Gaussian distribution of errors). The results will not
523 be valid if these assumptions are violated. Cen et al. (2010) recommended using data

524 transformation and weighting methods as a pre-processing approach before implementing the
525 inverse algorithm. Since the optical parameters are sensitive to the SR reflectance profile, high
526 noise level and improper selection of the profile region could result in large estimation errors. In
527 addition, for estimating the optical parameters of layered media, the increased number of free
528 parameters can dramatically increase the computational time, further exacerbating the estimation
529 of optical parameters, and/or causing ill-posed problems. Different strategies, such as a multi-
530 step method, sensitivity analysis and statistical evaluation, have been proposed to optimize the
531 inverse algorithms and improve the estimation accuracies (Cen et al., 2010; Hu et al., 2019;
532 Wang et al., 2017a; 2017b).

533 In contrast to the above inverse approach for estimating the optical absorption and scattering
534 coefficients of fruits and vegetables, researchers have also proposed several direct approaches to
535 characterize the obtained SR profiles for quality assessment of fruit and vegetables. With these
536 direct methods, the acquired SR profiles (usually after corrections for the dark and instrument
537 responses) are fitted with some empirical mathematical equations (e.g., Gaussian and Lorentzian
538 functions, etc.) (Peng and Lu, 2006, 2007) or by extracting image features (including mean
539 reflectance, image histogram, scattering size or area, etc.) from the 2-D scattering images (in the
540 cases of monochromatic or multispectral scattering images) (Qing et al., 2008; Lu, 2004;
541 Romano et al., 2011; Tu et al., 2000). While these direct methods are faster and simpler in
542 extracting the features from the SR profiles and also have yielded good results in predicting
543 quality of fruits and vegetables, they are highly dependent on type of instrumentation and light
544 source/detector setup.

545

546 3.3 *Time-resolved*

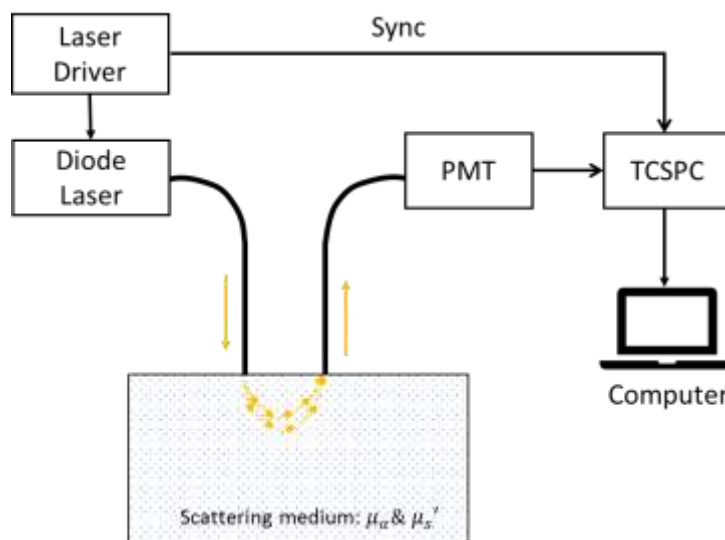
547 In TR technique, ultrashort laser pulses are injected into a turbid sample, and temporal
548 responses of the reemitted light at a certain distance away from the laser incident point are
549 recorded (Figure 1b). The temporal responses are a function of time. After acquisition of the
550 time-resolved reemitted light intensity signals, the absorption and reduced scattering coefficients
551 are then estimated by fitting the acquired TR data using an inverse algorithm for an analytical
552 solution for the diffusion equation.

553 3.3.1 *Instrumentation*

554 Figure 7 shows the schematic of a TR system for measuring optical properties of turbid
555 biological samples. The two key components for the TR system are a laser (or lasers for a
556 multiple wavelength system, or a tunable laser for a broad spectral region), which can generate
557 ultrashort pulses at the repetition frequency up to 100 MHz, and a time-correlated single photon
558 counting (TCSPC) device, which counts the number of photons arriving at the detector for
559 different time intervals. Hence, the detection system essentially records the histogram of the
560 detection times for the reemitted photons from the sample. To accurately measure the optical
561 properties of tissues, the TCSPC device needs to have the capability of providing sufficient time
562 resolution down to picoseconds (10^{-12} s) or even femtoseconds (10^{-15} s). A high temporal
563 resolution and high sensitivity are critical to the performance of a TR system. Temporal
564 resolution is related to both the width of laser pulses and the timing accuracy of the detection
565 electronics. To achieve high sensitivity, it is desirable to have a high-power laser (or lasers), but
566 a laser with excessive power can cause damage to biological tissues and pose safety concerns.
567 Hence, there is a delicate balance between sensitivity and safety in choosing an appropriate level
568 of laser power for a TR system. Over the years, many different TR techniques have been

569 developed for biomedical applications (Tuchin, 2007, Wang and Wu, 2007). Three TR
570 instrumentation configurations were developed by a group of researchers in Italy for measuring
571 the optical properties of biological tissues and horticultural products over a broad spectral range,
572 at a single wavelength, and at select discrete wavelengths (Rizzolo and Vanoli, 2016). TR
573 imaging systems have also been reported for 3-D imaging of biological tissues (Hebden et al.,
574 2004; Pifferi et al., 2003).

575 Compared to SR and SFD methods, the TR method is considered to be more accurate in
576 measuring optical properties and able to interrogate deeper tissues, which is important in
577 assessing quality and internal defects of horticultural products with a relatively thick surface
578 layer (i.e., skin or rind). However, TR techniques are expensive and complex, even for a portable
579 TR instrument. Moreover, it is important to have good contact of the detection probe with the
580 sample during the measurement, which may not be easy in working with intact fruit and
581 vegetable products of curved or irregular shape.



582

583 Figure 7. Schematic of a single-wavelength time-resolved system for measuring optical
584 properties of biological tissues, where PMT is a photomultiplier tube for detecting single photons

585 and TCSPC represents a time-correlated single photon counting device synchronized with the
586 laser driver.

587 *3.3.2 Data analysis*

588 In principle, once the temporal response curves have been obtained for samples, values of μ_a
589 and μ_s' can be obtained by fitting the data using a nonlinear inverse algorithm for an analytical
590 solution for the diffusion approximation equation (Patterson et al., 1989). However, like the case
591 discussed earlier for SR technique, due to the complex instrument response to optical signals, a
592 direct curve-fitting approach could result in large errors in the estimation of optical
593 parameters. Torricelli (2009) proposed to convolute the theoretical TR reflectance with the
594 instrument response function is first calculated, which is then used to fit the experimental TR
595 reflectance curve. According to Torricelli (2009), this approach yielded better results compared
596 to the approach of directly using the acquired TR data.

597

598 *3.4 Spatial-frequency domain*

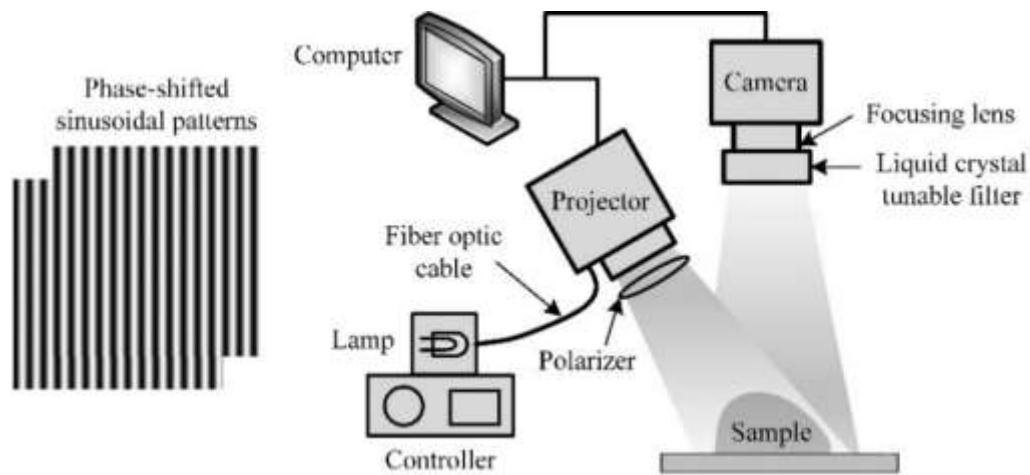
599 Spatial-frequency domain (SFD) technique was first reported by Cuccia et al. (2005) as a
600 means for estimating the optical absorption and scattering properties of turbid media. The
601 technique is different from SR and TR in that it allows wide-field mapping of optical properties
602 in turbid biological materials. Thus, it has the capability of 3-D imaging of biological tissues.
603 Instead of using a point light source for SR and TR techniques, SFD requires using special
604 patterns of 2-D illumination (usually sinusoidal patterns). To estimate the optical properties,
605 reflectance images are acquired from the sample with different spatial frequencies of
606 illumination, and the acquired images are then demodulated to obtain direct component (DC) and
607 alternating component (AC) images. The amplitudes of reflectance from the demodulated images

608 are then used for the inverse curve fitting by an analytical diffusion equation (Cuccia et al., 2009)
609 to obtain the estimated values of μ_a and μ_s' .

610 *3.4.1 Instrumentation*

611 Figure 8 shows the schematic of an SFD system for measuring optical properties of fruits and
612 food products. The system mainly consists of a high-performance CCD camera, a liquid crystal
613 tunable filter (LCTF), which allows selecting specific wavelengths for imaging, a polarizer that
614 blocks specular reflectance from the sample, and a digital light projector (DLP), which is
615 controlled by computer and connected to a DC light source via a fiber optic cable. The DLP can
616 generate different patterns of illumination through computer programming. For optical property
617 measurements, sinusoidal patterns of illumination are used to illuminate samples. For each
618 spatial frequency, three patterned images, corresponding to three phase-shifted sinusoidal
619 illumination patterns (120 degrees apart), are usually needed. To estimate the absorption and
620 reduced scattering coefficients, images should be acquired for a range of spatial frequencies. To
621 ensure accurate measurement of optical properties of turbid food samples, several calibration
622 procedures have to be carried out for an SFD system (Bodenschatz et al., 2014). First, it is
623 important that the camera system has good linearity responses. Second, under the ideal situation,
624 the illumination patterns should be sinusoidal. However, this may not always be realized due to
625 optical system imperfections and a specific setup of the light source. Hence, careful calibrations
626 should be done on standard reflectance panels (e.g., the reflectance panels by Labsphere, Inc.,
627 North Sutton, NH, USA). For the SFD setup configuration shown in Figure 8, the light
628 illumination is not incident onto the sample from the vertical or normal direction, which would
629 create nonuniform illumination on the sample and should thus be corrected. In addition, the light
630 illumination along the second axis should be constant in intensity, but in real situations, this may

631 not always be the case. Hence, careful calibration of the system is required to eliminate or
632 minimize these effects.

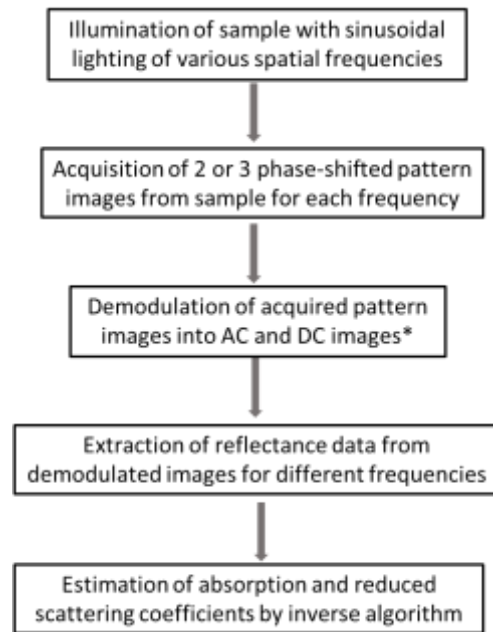


633
634 Figure 8. Schematic of a spatial-frequency domain imaging system for measuring optical
635 properties of horticultural products (Lu et al., 2016a).

636 3.4.2 Data analysis

637 Figure 9 shows a typical procedure for implementing the SFD technique for estimating
638 optical absorption and reduced scattering coefficients. First, two or three phase-shifted images
639 are acquired for each spatial frequency at each wavelength. The number of spatial frequencies
640 used varied in different studies; some used more than 12, while others only used a few (e.g., 4 to
641 6). The next step is to perform demodulation of the acquired pattern images, from which DC and
642 AC images are obtained. The conventional demodulation method requires three images, while
643 using new methods, such as spiral phase transform and Gram-Schmidt orthonormalization, two
644 patterned images would be enough (Lu et al., 2016b, 2016c). After the demodulation, the
645 reflectance values (the amplitude) are extracted. The extracted reflectance profile versus spatial
646 frequency is then fitted by the diffusion model with an appropriate inverse algorithm, from
647 which the absorption and reduced scattering coefficients are estimated for each wavelength. In

648 performing the inverse algorithm for curve fitting, one should be aware that the analytical
649 solution for the SFD method is derived based on two basic assumptions: 1) scattering is
650 dominant (i.e., $\mu_s \gg \mu_a$), and 2) the spatial frequency is much smaller than the transport
651 coefficient (i.e., $\mu_{tr} = \mu_a + \mu_s'$). Studies have shown that SFD technique is prone to errors due to
652 the complexity of the diffusion model and low signal-to-noise ratio for measured data at large
653 spatial frequencies. It is therefore important that proper inverse algorithm implementation
654 procedures are utilized, which include data smoothing, selection of proper spatial frequency
655 range and start and end frequencies. An SFD system consists of many optical components (lens,
656 tunable filter, detector, etc.), each of which has different optical response characteristics. The
657 optical response of the optical assembly will have important ramifications on the acquired
658 reflectance images. Hence, proper calibrations of the optical system are needed to reduce or
659 minimize errors in estimating the optical properties. Hu et al. (2019) suggested that the most
660 effective method for image correction is to use reference samples covering a range of known
661 properties to calibrate the acquired or demodulated reflectance images. Two-step and stepwise
662 optimization methods, including the reference-sample based correction procedure, were
663 proposed to improve the optical parameter estimation by SFD technique (Hu et al., 2018, 2019).



664

665 Figure 9. The procedure of implementing spatial-frequency domain technique for measuring
 666 optical properties of fruit and vegetable samples (* AC and DC denote amplitude and direct
 667 components, respectively).

668 So far, only limited studies have been reported on using SFD technique for optical
 669 characterization of fruits and vegetables, including apples, mangoes, and pears (Anderson et al.,
 670 2007; He et al., 2017, 2018; Hu et al., 2016).

671 Similar to SR technique, a direct approach for SFD technique, called structured-illumination
 672 reflectance imaging (SIRI), has been proposed as a new imaging modality for quality evaluation
 673 of horticultural products (Lu, 2018; Lu and Lu, 2017b; Lu et al., 2016a). The SIRI system shares
 674 the same optical configuration as that for the SFD system as shown in Figure 8, and the same
 675 demodulation procedure is used to obtain DC and AC images. Instead of using the inverse
 676 algorithm to estimate the optical absorption and reduced scattering coefficients, SIRI directly
 677 applies image processing procedures on the DC and AC images to extract image features for

678 evaluating quality of fruits and vegetables. Studies (Li, et al., 2018; Lu et al., 2017b) showed that
679 AC images, which are unique to the SIRI technique, provide higher spatial resolution and image
680 contrast and can reveal subsurface tissue features at specific depths, compared to DC images,
681 which are equivalent to the ones acquired under uniform, diffuse illumination. SIRI was found to
682 be especially useful for detecting subsurface defects (e.g., bruising in apples and tomatoes) and
683 early developments of fungal infection in peaches and other fruits (Sun et al., 2019), which are
684 difficult to ascertain by other conventional imaging techniques.

685

686 **4. Applications**

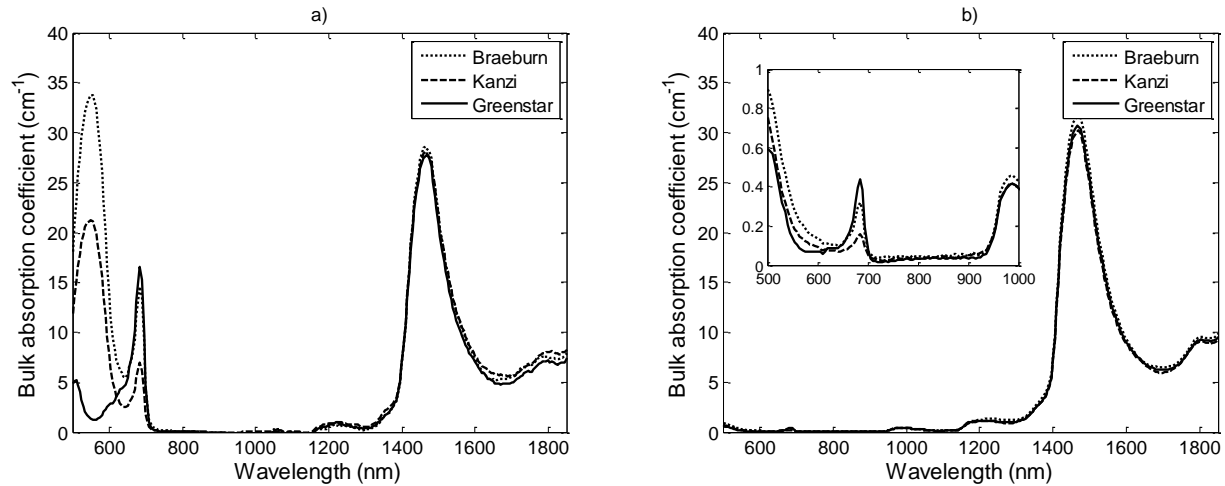
687 Considerable research has been reported in recent years on using IS-IAD, SR, TR and SFD
688 techniques to measure optical absorption and scattering properties of fruits and vegetables as
689 well as on using these optical properties for maturity and quality assessment and for disease and
690 defect detection. As discussed in Section 3, direct approaches for analyzing SR and SFD signals
691 also have been proposed for evaluating quality of horticultural and food products. However, our
692 discussion in this section is mainly focused on the application of optical absorption and
693 scattering properties for quality assessment of fruits and vegetables.

694 *4.1 Absorption and scattering spectra for fruits and vegetables*

695 Figure 10 shows typical mean absorption coefficient (μ_a) spectra for the apple skin (Figure
696 10a) and cortex tissues (Figure 10b) of three apple cultivars ('Braeburn', 'Greenstar', and
697 'Kanzi') in the spectral region of 500-1850 nm, which were measured using an IS-IAD technique
698 (Van Beers et al., 2017b). The insert in Figure 10b shows a close-up of the absorption coefficient
699 for the apple cortex in the 500-1000 nm region. Several absorption peaks are observed for the

700 apple skin over the visible region of 550-680 nm, which are attributed to carotenoids (around 500
701 nm), anthocyanins (550 nm – 600 nm) and chlorophyll (mainly chlorophyll a at 678 nm).
702 Absorption peaks around 678 nm are also noticed for the apple cortex; however, their values are
703 at least 10 times smaller than those for the apple skin, which indicates the presence of
704 chlorophyll and carotenoids, albeit at much lower concentration levels, in the apple cortex. In
705 addition, the OH bonds in water also have an important effect on the absorption coefficient for
706 both apple skin and cortex in the NIR region around 970 nm, 1200 nm and 1450 nm (Hale and
707 Querry, 1973; Lancaster et al., 1994; Merzlyak et al., 2003). Differences between the cultivars
708 can also be observed. For example, absorption at 550 nm is much lower for ‘Greenstar’, a green
709 cultivar with little anthocyanins in the skin.

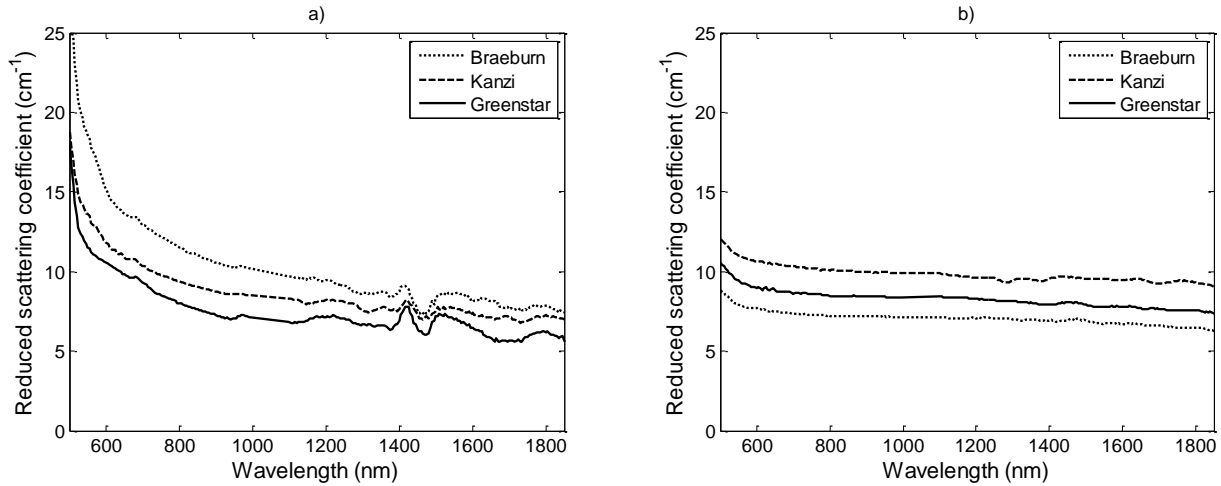
710 Absorption spectra reported for other fruit and vegetables (apple, blueberry, kiwifruit,
711 mango, onion, peach, pear, pickling cucumber, plum, tomato, zucchini squash) are also largely
712 dominated by water in the NIR range and chromophores like chlorophyll, carotenoids and
713 anthocyanins in the visible range (Cen et al, 2012; Cen et al., 2013; Cubbedu et al., 2001; Huang
714 et al., 2018b; Lu et al., 2011; Nguyen Do Trong et al., 2014; Nicolai et al., 2008; Qin and Lu,
715 2008; Saeys et al., 2008; Spinelli et al., 2012; Vanoli et al., 2011; Wang et al., 2014; Zhang et al.,
716 2017a). For example, in immature tomatoes (i.e., in the green and breaker stages) chlorophyll
717 dominates the visible spectral region, while for ripe, red tomatoes, chlorophyll disappears, and
718 carotenoids (mainly lycopene) increase significantly (Clément et al., 2008; Huang et al., 2018).



719

720 Figure 10. Mean absorption coefficients of the apple skin (a) and cortex (b) tissues of three apple
 721 cultivars (Van Beers et al., 2017b).

722 The mean reduced scattering coefficient (μ_s') spectra for the apple skin and cortex tissues of
 723 the same three cultivars are illustrated in Figure 11 (Van Beers et al., 2017b). The reduced
 724 scattering coefficient decreases exponentially with the increasing wavelength, which is typical
 725 for biological tissues (Bashkatov et al., 2005). Again, differences are noticed between the
 726 different cultivars and between the tissue types. These differences in the scattering behavior
 727 typically relate to differences in the microstructure, like differences in the cell structure and
 728 porosity in both tissue types. Other researchers also reported μ_s' values for different fruits,
 729 ranging between 0 cm^{-1} and 20 cm^{-1} (Cen et al., 2012, 2013; Huang et al., 2018; Nguyen Do
 730 Trong et al., 2014; Qin and Lu, 2008; Rowe et al., 2014; Saeys et al., 2008; Seifert et al., 2015).



731

732 Figure 11. Mean reduced scattering coefficients of the (a) skin and (b) cortex tissue of three
 733 apple cultivars (Van Beers et al., 2017b).

734 In studying the effect of pre-harvest maturation on the optical properties, Van Beers *et al.*
 735 (2017b) found significant changes in the optical behavior of the apple tissues. The absorption by
 736 anthocyanins was found to increase, while the scattering coefficients (μ_s) of the apple cortex
 737 decreased. It was hypothesized that this evolution in scattering could be related to cell elongation
 738 during maturation, reducing the volume fraction of cell walls and air pores encountered by the
 739 light (Van Beers et al., 2017b).

740 In studying the effect of bruising on the absorption and scattering properties of apples over
 741 time, Lu et al. (2010) reported that while no consistent pattern of changes in the absorption
 742 spectra over time was observed, there was, however, a steady decreasing trend in the values of
 743 μ_s' over time. A similar trend of changes in the absorption and reduced scattering coefficients for
 744 the spectral region of 950-1400 nm was also reported for healthy and bruised blueberries when
 745 IS-IAD was employed (Zhang et al., 2017a). These studies suggested that bruise detection could
 746 be enhanced by utilizing the scattering properties of fruit. Wang et al. (2014) measured the

747 absorption and reduced scattering coefficients for healthy and diseased onion tissues in the
748 spectral region of 550-1650 nm. They reported that values of the reduced scattering coefficient
749 for dry skin were 10 times higher than that of onion flesh. Likewise, large differences in the
750 absorption coefficient values over the spectral region of 550-1300 nm were observed between
751 dry skin and flesh onion tissues.

752 4.2 *Maturity and quality assessment*

753 Maturity determines when fruits or vegetables should be harvested and how they should be
754 stored or marketed after harvesting. Maturity directly influences postharvest quality and shelf life
755 of horticultural products. Hence, nondestructive measurement of product maturity before and at
756 harvest is critical for the fruit and vegetable industries. Generally, maturity assessment requires
757 measuring multiple quality attributes. Different fruits and vegetables may have different
758 requirements or standards for assessing maturity. For instance, in assessing the maturity of
759 apples, multiple quality parameters, including fruit surface color, soluble solids content (SSC),
760 starch pattern index, flesh firmness and even titratable acidity, are often used. On the other hand,
761 tomato maturity is mainly judged based on the surface or flesh color distributions, upon which
762 tomatoes are classified into six maturity or ripeness grades. The maturation of fruits or
763 vegetables is accompanied with changes in the chemical composition and structural
764 characteristics. Consequently, the absorption and scattering properties also change during the
765 maturation process, although the trend and magnitude of changes for the two optical properties
766 are different. Hence, optical absorption and reduced scattering coefficients are useful for
767 assessing multiple maturity parameters of fruits and vegetables. Table 1 lists some recent studies
768 on assessing maturity and quality of fruits and vegetables, including apple, banana, kiwifruit,
769 mango, nectarine, peach, pear, plum and tomato, by using IS-IAD, SR, TR and SFD techniques.

770 Not surprising, most studies were focused on using the two optical parameters measured by SR
771 and TR techniques to predict firmness and SSC, the two most important quality attributes for a
772 variety of fruits. These studies have demonstrated that both absorption and reduced scattering
773 coefficients were related to firmness, SSC, flesh color, and starch index. However, the absorption
774 coefficient overall was better for predicting these quality parameters, which could be attributed
775 to the fact that pigments and other chemical composition change during maturation,
776 accompanied with changes in the cellular structures. In most cases, it was also found that
777 combination of the two optical parameters tended to improve predictions of the fruit
778 maturity/quality parameters (Barzaghi et al., 2009; Cen et al., 2012; Huang et al., 2018a, 2018b;
779 Qin and Lu, 2009; Vanoli et al., 2011). However, Nguyen Do Trong et al. (2014a) reported the
780 best results for SSC prediction based on the absorption coefficient spectra. While few studies
781 have been reported on directly comparing the performance of SR and TR techniques with
782 conventional Vis/NIR spectroscopy, the overall results appeared to be comparable between the
783 two approaches (Barzaghi et al., 2009; Huang et al., 2018a, 2018b). The current optical
784 measurement techniques are still prone to errors in data acquisition as well as during the inverse
785 algorithm extraction of optical parameters, thus preventing them from achieving full potential in
786 assessing maturity and quality of fruits and vegetables.

787 The softening of apples during postharvest storage is often accompanied with the structural
788 changes in the fruit tissues and their optical properties. In studying the relationship between the
789 optical properties of apples and the cell structures and firmness, Cen et al. (2013) reported that
790 during the accelerated softening of apples at room temperature, the reduced scattering coefficient
791 for the measured apples of ‘Golden Delicious’ and ‘Granny Smith’ varieties for the spectral
792 region of 500-800 nm showed a consistent pattern of decrease over a period of 30 days, while the

793 change of the absorption coefficient was more complex. They further reported that the absorption
 794 and reduced scattering coefficients at 675 nm, which corresponds to chlorophyll absorption, were
 795 strongly correlated with tissue firmness as well as the area or diameter of tissue cells. This is
 796 because the decrease of firmness during the accelerated softening is also accompanied with a
 797 decrease in the chlorophyll content. Eccher Zerbini et al. (2006, 2011, 2015) developed
 798 mathematical models relating the softening of apples, mangoes, and nectarines with the
 799 absorption coefficient at 540 nm and 670 nm.

800 In using a SR sensing probe to measure the optical properties of dried apple slices, Nguyen
 801 Do Trong et al. (2014b) reported that the scattering coefficient was related to the processing
 802 condition, microstructure and textural quality. Rizzolo et al. (2011; 2014b) also reported that the
 803 absorption coefficient of ‘Cripps Pink’ and ‘Golden Delicious’ apples at 670 nm measured at
 804 harvest could be used to classify raw and dried apple rings for different quality grades.

805 Table 1. Assessment of maturity and postharvest quality of fruits and vegetables by using
 806 optical measurement techniques

Product	Maturity/Quality Parameter*	Measuring Technique**	Reference
Apple (Fresh)	Firmness, SSC, anthocyanins, chlorophyll, carotenoids, starch index, softening, sensory profile	IS, SR, TR	Barzaghi et al. (2009); Cen et al. (2013); Nguyen Do Trong et al. (2014a); Qin et al. (2009); Rizzolo et al. (2010b, 2014a); Sun et al. (2017); Van Beers et al. (2017b); Vanoli et al. (2011, 2015)
Apple (dried or processed)	Hardness, firmness, elasticity, crispness, snapping work, browning index, flesh color, porosity	SR, TR	Nguyen Do Trong et al. (2014b); Rizzolo et al. (2011, 2014b)
Banana	Firmness, SSC, ripeness	SR	Adebayo et al. (2016)
Kiwifruit	Firmness, SSC, acidity	TR	Valero et al. (2004)
Mango	Firmness, pulp color, softening	TR	Eccher Zerbini et al. (2015); Pereira et al. (2010); Spinelli et al., (2012)
Nectarine	Firmness, softening	TR	Eccher Zerbini et al. (2006, 2011); Rizzolo et al. (2010a); Tijskens et al. (2007a, 2007b)
Peach	Firmness, SSC	SR, TR	Cen et al. (2012b); Rizzolo et al. (2013)

Pear	Firmness, SSC, softening	IS, SR, TR	Adebayo et al. (2017); He et al. (2016); Nicolai et al. (2008);
Tomato	Firmness, SSC, surface color, flesh color, ripeness	SR	Huang et al. (2018); Qin and Lu (2008); Zhu et al. (2015)

807 * SSC =soluble solids content. ** IS=integrating sphere, SR=spatially resolved, SFD=spatial-frequency domain,
808 TR=time-resolved.

809

810 4.3 Defect detection

811 Fresh fruits and vegetables are susceptible to a variety of physiological and pathological
812 disorders and mechanical damage during growth, harvest and postharvest handling and storage.
813 Surface defects are relatively easy to detect, while many internal defects still cannot be
814 effectively detected by using the existing optical techniques. Products with defects, either
815 external or internal, tend to have poor marketability and could be rejected by consumers. Hence,
816 it is critical that defective fresh products, especially those with internal defects, be removed or
817 separated during postharvest packing operations. Over the years, many optical techniques (e.g.,
818 Vis/NIR, fluorescence imaging, hyper- and multi-spectral imaging, X-ray imaging, and magnetic
819 resonance imaging) have been used for detecting defects of fruits and vegetables (Lu et al., 2017;
820 Lu and Lu, 2017). For instance, Vis/NIR spectroscopy is now being used in some fruit
821 packinghouses for detecting and segregating fruit with internal defect. However, the commercial
822 Vis/NIR systems still cannot fully meet industry needs because of high false positive/negative
823 rates. Hence, new, more effective inspection technologies are especially needed for internal
824 defect detection.

825 Physiological disorders often cause changes in the chemical and structural properties of
826 products, which would subsequently induce changes in the optical absorption and scattering
827 properties. For instance, internal browning is a common symptom for apple and many other
828 fruits. Apples with internal browning were found to have higher values for the absorption

829 coefficient at 750 nm and lower values for the reduced scattering coefficient at the same
830 wavelength (Vanoli et al., 2009). Due to its ability of penetrating tissues at greater depth, TS
831 technique has been used to detect internal browning and/or internal bleeding of apples,
832 nectarines, and plums (Lurie et al., 2011; Vangdal et al., 2012; Vanoli et al., 2009, 2012).
833 Mealiness alters the cellulosic structure of apple tissues and hence the optical properties. It was
834 thus feasible to differentiate mealy apples from normal ones based on the absorption and reduced
835 scattering coefficients (Vanoli et al., 2009). Likewise, water-cored apples were found to have
836 higher values for the absorption coefficient at 790 nm and lower values for the reduced scattering
837 coefficient (Vanoli et al., 2009). Studies also showed that diseased onions showed significantly
838 different absorption and scattering characteristics compared to normal onion tissues (Wang et al.,
839 2014). Table 2 lists some recent studies on using the various optical measuring techniques for
840 detecting defects for a variety of fruits and vegetables. While these studies have demonstrated
841 that absorption and reduce scattering coefficients can be used for differentiating normal and
842 defective tissues, there still exist considerable challenges in implementing SR, TR or SFD for
843 real-time, practical inspection of fruits and vegetables for internal defects. First, these techniques
844 are still too slow to be suitable for real-time sorting and grading. Second, both SR and TR
845 techniques are not suitable for detecting defects that are localized or deep inside fruit or
846 vegetable products. TR technique allows greater penetration of light into tissues, but its
847 measurement can only interrogate a small section of the sample tissue. While SFD technique has
848 potential for wide-area, 3D mapping of optical properties for horticultural products, it has limited
849 capabilities of imaging tissues at no more than 1-2 mm deep.

850 Table 2. Detection of defects of fruits and vegetables using optical absorption and scattering
851 properties.

Product	Type of Defect	Measuring Technique*	Reference
----------------	-----------------------	-----------------------------	------------------

Apple	Bruising	IS, SR, SFD	Anderson et al., (2007); Lu et al. (2010); Zhang et al. (2017b)
	Internal browning	SFD, TR	Hu et al. (2016); Lurie et al. (2011); Vanoli et al. (2009, 2012);
	Mealiness	TR	Valero et al. (2005); Vanoli et al. (2009)
	Watercore	TR	Vanoli et al. (2009)
Blueberry	Bruising	IS	Zhang et al. (2017a, 2019)
Cucumber (pickling)	Bruising	SR	Lu et al. (2011)
Nectarine	Internal bleeding, internal browning	TR	Lurie et al. (2011)
Onion	Sour skin, neck rot	IS	Wang et al. (2014)
Orange	Decay	SR	Lorente et al. (2015)
Pear	Brown heart	TR	Eccher Zerbini et al. (2002)
Plum	Internal browning	TR	Vangdal et al. (2012)

852 * IS=integrating sphere, SR=spatially resolved, SFD=spatial-frequency domain, TR=time-resolved.

853

854 5. Issues and Challenges

855 Over the past 15 years, we have seen significant research efforts in the development and
856 application of new SR, SFD, and TR techniques, along with IS-IAD, for optical characterization
857 of horticultural and food products. While these emerging techniques offer new opportunities for
858 quality and safety assessment of horticultural and food products, there still exist considerable
859 issues and challenges in using these techniques due to increased sophistication and investment in
860 instrumentation and algorithms, compared to conventional spectroscopic techniques. First, many
861 of these techniques are based on the diffusion approximation theory (except for data-based
862 models or MC libraries discussed in Section 2). As discussed earlier, the diffusion approximation
863 theory is only applicable to samples, in which light scattering is dominant over absorption (i.e.,
864 $\mu_s \gg \mu_a$). This condition is not always met satisfactorily as many biological materials like fruits
865 and vegetables show strong absorption at specific wavelengths or spectral regions due to

866 biological chromophores (anthocyanins, carotenoids, chlorophyll, water, etc.). For these spectral
867 regions, the diffusion theory would introduce large errors or is completely inadequate. Second,
868 accurate estimations of optical absorption and scattering properties are also hindered by our
869 ability of acquiring reliable, high-quality spatially- or time-resolved reflectance signals from
870 horticultural samples, which are sensitive to noise and imperfect sample conditions (e.g.,
871 irregular geometry, limited sample dimensions, presence of local defects or abnormalities, etc.).
872 With SR techniques, a small, collimated, and normally-incident light source is critical to proper
873 measurement of spatially-resolved reflectance. However, it is difficult to meet all the
874 requirements in actual application situations. Likewise, with TR techniques, the equipment used
875 to generate short laser pulses and acquire the reflected signals over the time scale of 10^{-12} s to 10^{-9}
876 s are complex and expensive. Accurate measurements of optical properties are further
877 complicated by the fact that many fruits and vegetables are heterogeneous in structure and are of
878 irregular shape or uneven surface. Specifically, the surface layer (i.e., skin or rind) of
879 horticultural products has distinct optical properties and its presence could cause problems for
880 the measurement of sublayer optical properties, which are usually of major interest for quality
881 assessment (Saeys et al., 2008; Van Beers et al., 2017b). Hence, it is desirable or even necessary
882 to consider the heterogeneity properties in measuring fruit and vegetable products. Preliminary
883 efforts have been made on using SR and SFD techniques to measure the optical properties of
884 fruit skin and flesh by treating them as two layers of homogeneous tissues (Cen and Lu, 2009;
885 Hu et al., 2019; Wang et al., 2017a). However, considerably more challenges would be
886 encountered in obtaining acceptable estimations of the optical properties of individual layers, due
887 to the increased number of unknown optical parameters and much more complicated
888 mathematical models for two-layer turbid media. Moreover, in all SR, TR and SFD systems, the

889 acquired reflectance signals are closely related to the instrument response. It is thus important
890 that the reflectance signals be properly corrected or calibrated, before being used for inverse
891 estimation of optical properties. Currently, no standard procedures have been established for
892 calibrating these optical systems. Consequently, the optical measurement results are influenced,
893 to a great extent, by the calibration procedure. Many a time, reference samples of known optical
894 properties are needed during the calibration process. Proper procedures for preparation and
895 selection of reference samples are thus critical to the calibration of an optical system.

896 Furthermore, many SR, TR and SFD measurement configurations require contact of the light
897 source and/or detection probe with the sample to be measured. The measurements are not carried
898 out in real time and/or rapidly. For horticultural and food products, fast and noncontact
899 measurements are often needed or desirable. Hence, much research is still needed in further
900 development and/or improvement of these emerging optical property measurement techniques
901 for better assessment of horticultural and food products. Finally, proper preprocessing
902 procedures for the acquired reflectance data are important for the inverse estimation of optical
903 parameters. Different preprocessing treatment methods and procedures can have significant
904 ramifications on the estimation of optical parameters (Cen and Lu, 2010, 2011; Hu et al., 2018,
905 2019; Wang et al., 2017a, 2017b).

906 Overall, the inverse approach to optical property estimation is a complicated process, and it
907 relies on an appropriate mathematical model, precise instrumentation setup and calibrations, and
908 rigorous inverse algorithms. Large estimation errors for the optical parameters could be incurred,
909 if the measuring system is not carefully calibrated, procedures for the inverse algorithm are not
910 properly implemented, or samples are of irregular shape or contain defective or irregular tissue
911 spots within the area of measurement. The presence of these issues and challenges also provides

912 opportunities for further research for these emerging techniques. Further research should also be
913 directed at the development of low-cost, portable or even miniaturized optical measuring systems
914 that can perform optical property measurements in real time, in the field, and under online
915 situations.

916 In view of the more complicated, time-consuming procedures for inverse estimation of the
917 optical properties, researchers have also proposed simpler and faster direct approaches to analyze
918 the reflectance data acquired from SR and SFD techniques for quality and maturity assessment
919 and defect detection of fruits and vegetables. For instance, simple empirical mathematical
920 models or scattering image features have been used to describe the 1-D scattering profiles or 2-D
921 scattering images acquired by SR technique in FOP (Huang et al., 2018c), MCI (Baranyai and
922 Zude, 2009; Lu, 2004; Mollazade et al., 2013; Peng and Lu, 2005, 2006; Qing et al., 2008), or
923 HSI modes (Huang and Lu, 210; Peng and Lu, 2008), which were found to correlate well with
924 quality attributes such as fruit firmness and SSC. For the SFD technique, SIRI has been used as a
925 new imaging modality for detecting subsurface defects of apple, peach, and other fruits (Li et al.,
926 2018; Lu et al., 2016a; Lu and Lu, 2017; Sun et al., 2019). However, these direct approaches are
927 highly dependent on instrumentation setup and the models developed for different systems are
928 generally not interchangeable and cannot be compared directly for different studies.

929 **6. Conclusions**

930 Optical absorption and scattering properties are directly related to the chemical and structural
931 properties of fruits and vegetables, and thus are useful for evaluating maturity, quality and
932 defects of products. Over the past 15 years, several emerging optical property measuring
933 techniques have been made available for assessing fruits and vegetables and other food products.
934 IS-IAD technique is widely used as a standard method for measuring optical absorption and

935 scattering properties. The technique is, however, destructive and requires careful preparation of
936 samples with specific dimensions for measurement. SR technique is relatively simple in
937 instrumentation, low in cost and faster in measurement. Thus, different SR sensing
938 configurations have been developed for measuring fruits and vegetables. However, accurate
939 estimation of optical absorption and reduced scattering coefficients by SR technique is still
940 challenging, due to measurement errors in SR reflectance and challenges in the inverse algorithm
941 implementation. TR technique, on the other hand, can interrogate tissues at greater depth, which
942 is important for detection of internal quality or defects in horticultural products. However, the
943 technique needs sophisticated and expensive instrumentation, which could limit it for wide
944 practical applications in quality inspection of fruits and vegetables. SFD technique offers the
945 unparalleled capability and potential of measuring and mapping optical properties of fruit and
946 vegetable products, but its imaging depth and resolution is still limited. Considerable research is
947 thus needed in both hardware and software (i.e., mathematical modeling and data processing) for
948 improving accuracy and reliability in measurement of the optical properties by these emerging
949 optical techniques. Moreover, research should also be devoted to the development of low-cost,
950 portable or miniaturized optical property measurement systems and for implementing these
951 emerging techniques for real-time, online applications for quality assessment of horticultural
952 products.

953 **References**

- 954 Adebayo, S.E., Hashim, N., Abdan, K., Hanafi, M., Mollazade, K., 2016. Prediction of quality
 955 attributes and ripeness classification of bananas using optical properties. *Scientia Hort.* 212,
 956 171-182.
- 957 Adebayo, S.E., Hashim, N., Reich, O., Regen, C., Munzberg, M., Abdan, K., Zude-Sasse, M.,
 958 2017. Using absorption and reduced scattering coefficients for non-destructive analyses of
 959 fruit flesh firmness and soluble solids content in pear (*Pyrus communis* 'Conference') – An
 960 update when using diffusion theory. *Postharvest Biol. Technol.* 130, 56-63.
- 961 Aernouts, B., 2014. Optical Characterization of Milk. Ph.D. thesis, KU Leuven, Belgium.
- 962 Aernouts, B., Erkinbaev, C., Watté, R., Van Beers, R., Nguyen Do Trong, N., Nicolai, B., Saeys,
 963 W., 2015. Estimation of bulk optical properties of turbid media from hyperspectral scatter
 964 imaging measurements: metamodeling approach. *Opt. Express* 23, 26049-26063.
- 965 Aernouts, B., Watté, R., Van Beers, R., Delport, F., Merchiers, M., De Block, J., Lammertyn, J.,
 966 Saeys, W., 2014. Flexible tool for simulating the bulk optical properties of polydisperse
 967 spherical particles in an absorbing host: Experimental validation. *Opt. Express* 22, 20223-
 968 20238.
- 969 Aernouts, B., Zamora-Rojas, E., Van Beers, R., Watté, R., Wang, L., Tsuta, M., Lammertyn, J.,
 970 Saeys, W., 2013. Supercontinuum laser based optical characterization of Intralipid®
 971 phantoms in the 500-2250 nm range. *Opt. Express* 26, 32450-32467.
- 972 Anderson, E.R., Cuccia, D.J., Durkin, A.J., 2007. Detection of bruises on Golden Delicious
 973 apples using spatial-frequency-domain imaging. *Proceedings of the SPIE* 6430, 64301O,
 974 SPIE, Bellingham, WA, USA.
- 975 Baranyai, L., Zude, M., 2009. Analysis of laser light propagation in kiwifruit using
 976 backscattering imaging and Monte Carlo simulation. *Comput. Electron. Agric.* 69, 33-39.
- 977 Barzaghi, S., Vanoli, M., Cremonesi, K., Cotellino, G., Torreggiani, D., Rizzolo, A., Grassi, M.,
 978 Spinelli, L., Torricelli, A., 2009. Outer product analysis applied to time-resolved reflectance
 979 spectroscopy (TRS) and NIR reflectance spectra of apples. *Proceedings of 14th International
 980 Conference on NIR Spectroscopy* 213-218. IM Publications LLP, Chichester.
- 981 Bashkatov, A.N., Genina, E.A., Kochubey, V.I., Tuchin, V.V., 2005. Optical properties of
 982 human skin, subcutaneous and mucous tissues in the wavelength range from 400 to 2000 nm.
 983 *Journal of Physics D: Applied Physics*, 38, 2543–2555.
- 984 Birth, G.S., 1978. The light scattering properties of foods. *J. Food Sci.* 16, 916-925.
- 985 Birth, G.S., 1982. Diffuse thickness as a measure of light scattering. *Appl. Spectros.*, 36, 675-
 986 682.
- 987 Birth, G.S., Davis, C.E., Townsend, W.E., 1978. The scatter coefficient as a measure of pork
 988 quality. *J. Animal Sci.* 46, 639-645.
- 989 Bodenschatz, N., Brandes, A., Liemert, A., Kienle, A., 2014. Sources of errors in spatial
 990 frequency domain imaging of scattering media. *J. Biomed. Opt.* 19, 071405.
- 991 Cen, H., Lu, R., 2009. Quantification of the optical properties of two-layer turbid materials using
 992 a hyperspectral imaging-based spatially-resolved technique. *Appl. Opt.* 48, 5612-5623.
- 993 Cen, H., Lu, R., 2010. Optimization of the hyperspectral imaging-based spatially-resolved
 994 system for measuring the optical properties of biological materials. *Opt. Express* 18, 17412-
 995 17432.

- 996 Cen, H., Lu, R., Dolan, K., 2010. Optimization of inverse algorithm for estimating optical
 997 properties of biological materials using spatially-resolved diffuse reflectance. *Inverse Prob.*
 998 *Sci. Eng.* 18, 853-872.
- 999 Cen, H., Lu, R., Mendoza, F., 2012a. Analysis of absorption and scattering spectra for assessing
 1000 the internal quality of apple fruit. *Acta Hort.* 945, 181-188.
- 1001 Cen, H., Lu, R., Mendoza, F.A., Ariana, D.P., 2012b. Assessing multiple quality attributes of
 1002 peaches using optical absorption and scattering properties. *Trans. ASABE* 55, 647-657.
- 1003 Cen, H., Lu, R., Mendoza, F., Beaudry, R.M., 2013. Relationship of the optical absorption and
 1004 scattering properties with mechanical and structural properties of apple tissue. *Postharvest*
 1005 *Biol. Technol.* 85, 30-38.
- 1006 Clément, A., Dorais, M., Vernon, M., 2008. Nondestructive measurement of fresh tomato
 1007 lycopene content and other physicochemical characteristics using visible–NIR spectroscopy.
 1008 *J. Agric. Food Chem.* 56, 9813–9818.
- 1009 Cubeddu, R., D’Andrea, C., Pifferi, A., Taroni, P., Torricelli, A., Valentini, G., Dover, C.,
 1010 Johnson, D., Ruiz-Altisent, M., Valero, C., 2001a. Nondestructive quantification of chemical
 1011 and physical properties of fruits by time-resolved reflectance spectroscopy in the wavelength
 1012 range of 650-1000 nm. *Appl. Opt.* 40, 538-543.
- 1013 Cubeddu, R., D’Andrea, C., Pifferi, A., Taroni, P., Torricelli, A., Valentini, G., Ruiz-Altisent,
 1014 M., Valero, C., Ortiz, C., Dover, C., Johnson, D., 2001b. Time-resolved reflectance
 1015 spectroscopy applied to the nondestructive monitoring of the internal optical properties in
 1016 apples. *Appl. Spectros.* 55, 1368-1374.
- 1017 Cuccia, D.J., Bevilacqua, F., Durkin, A.J., Tromberg, B.J., 2005. Modulated imaging:
 1018 quantitative analysis and tomography of turbid media in the spatial-frequency domain. *Opt.*
 1019 *Lett.* 30, 1354-1356.
- 1020 Cuccia, D.J., Bevilacqua, F., Durkin, A.J., Ayers, F.R., Tromberg, B.J., 2009. Quantitation and
 1021 mapping of tissue optical properties using modulated imaging. *J. Biomed. Opt.* 14, 024012.
- 1022 Doornbos, R.M., Lang, R., Aalders, M.C., Cross, F.W., Sterenborg, H., 1999. The determination
 1023 of in vivo human tissue optical properties and absolute chromophore concentrations using
 1024 spatially resolved steady-state diffuse reflectance spectroscopy. *Phys. Med. Biol.* 44, 967-
 1025 981.
- 1026 Du, H., Voss, K.J., 2004. Effects of point-spread function on calibration and radiometric
 1027 accuracy of CCD camera. *Appl. Opt.* 43, 665-670.
- 1028 Eccher Zerbini, P., Grassi, M., Cubeddu, R., Pifferi, A., Torrecilli, A., 2002. Nondestructive
 1029 detection of brown heart in pears by time-resolved reflectance spectroscopy. *Postharvest*
 1030 *Biol. Technol.* 25, 87-97.
- 1031 Eccher Zerbini, P., Vanoli, M., Grassi, M., Rizzolo, A., Fibiani, M., Cubeddu, R., Pifferi, A.,
 1032 Spinelli, L., Torricelli, A., 2006. A model for the softening of nectarines based on sorting
 1033 fruit at harvest by time-resolved reflectance spectroscopy. *Postharvest Biol. Technol.* 39,
 1034 223-232.
- 1035 Eccher Zerbini, P., Vanoli, M., Lovati, F., Spinelli, L., Torricelli, A., Rizzolo, A., Lurie, S.,
 1036 2011. Maturity assessment at harvest and prediction of softening in a late maturing nectarine
 1037 cultivar after cold storage. *Postharvest Biol. Technol.* 62, 275-281.
- 1038 Eccher Zerbini, P., Vanoli, M., Rizzolo, A., Grassi, M., de Azevedo Pimentel, R.M., Spinelli, L.,
 1039 Torricelli, A., 2015. Optical properties, ethylene production and softening in mango fruit.
 1040 *Postharvest Biol. Technol.* 101, 58-65.

1041 Erkinbaev, C., Herremans, E., Nguyen Do Trong, N., Jakubczyk, E., Verboven, P., Nicolai, B.,
1042 Saeys, W., 2014. Contactless and non-destructive differentiation of microstructures of sugar
1043 foams by hyperspectral scatter imaging. *Innov. Food Sci. Emerg. Technol.* 24, 131-137.

1044 Fabbri, F., Franceschini, M.A., Fantini, S., 2003. Characterization of spatial and temporal
1045 variations in the optical properties of tissuelike media with diffuse reflectance imaging. *Appl.*
1046 *Opt.* 42, 3063-3072.

1047 Fang, Z.H., Fu, X.P., He, X.M., 2016. Investigation of absorption and scattering characteristics
1048 of kiwifruit tissue using a single integrating sphere system. *J. Zhejiang Univ.-SCIENCE B*
1049 17, 484-492.

1050 Farrell, T.J., Patterson, M.S., Wilson, B., 1992. A diffusion theory model of spatially resolved,
1051 steady-state diffuse reflectance for the noninvasive determination of tissue optical properties
1052 in vivo. *Med. Phys.* 19, 879–888.

1053 Hale, G.M., Querry, M.R., 1973. Optical constants of water in the 200-nm to 200- μ m
1054 wavelength region. *Appl. Optics* 12, 555–563.

1055 Hjalmarsson, P., Thennadil, S.N. 2007. Spatially resolved in vivo measurement system for
1056 estimating the optical properties of tissue in the wavelength range 1000-1700 nm. In:
1057 Schweitzer, D., Fitzmaurice, M. (Eds.). *Proceedings of SPIE* 6628, 662805.

1058 Hjalmarsson, P., Thennadil, S. N. 2008. Determination of glucose concentration in tissue-like
1059 material using spatially resolved steady-state diffuse reflectance spectroscopy. In: Tuchin,
1060 V.V., Wang, L.V. (Eds.). *Proceedings of SPIE* 6855, 685508.

1061 He, X., Fu, X., Li, T., Rao, X., 2018. Spatial frequency domain imaging for detecting bruises of
1062 pears. *J. Food Meas. Charact.* 12, 1266-1273.

1063 He, X., Fu, X., Rao, X., Fu, F., 2017. Nondestructive determination of optical properties of a
1064 pear using spatial frequency domain imaging combined with phase-measuring profilometry.
1065 *Appl. Opt.* 56, 8207-8215.

1066 He, X., Fu, X., Rao, X., Fang, Z., 2016. Assessing firmness and SSC of pears based on
1067 absorption and scattering properties using an automatic integrating sphere system from 400
1068 to 1150 nm. *Postharvest Biol. Technol.* 121, 62-70.

1069 Hebden, J.C., Gibson, A., Austin, T., Yusof, R.M., Everdell, N., Delpy, D.T., Arridge, S.R.,
1070 Meek, J. H., Wyatt, J.S., 2004. Imaging changes in blood volume and oxygenation in the
1071 newborn infant brain using three-dimensional optical tomography. *Phys. Med. Biol.* 49,
1072 1117-1130.

1073 Hu, D., Fu, X., He, X., Ying, Y., 2016. Noncontact and wide-field characterization of the
1074 absorption and scattering properties of apple fruit using spatial-frequency domain imaging.
1075 *Sci. Rep.* 6, 37920.

1076 Hu, D., Lu, R., Ying, Y., 2018. A two-step parameter optimization algorithm for improving
1077 estimation of optical properties using spatial frequency domain imaging. *J. Quan. Spec. Rad.*
1078 *Transfer* 207, 32-40.

1079 Hu, D., Lu, R., Ying, Y., 2019. A stepwise method for estimating optical properties of two-layer
1080 turbid media from spatial-frequency domain reflectance. *Opt. Express* 27, 1124-1141.

1081 Huang, M., Lu, R., 2010. Optimal wavelength selection for hyperspectral scattering prediction of
1082 apple firmness and soluble solids content. *Trans. ASABE* 53, 1175-1182.

1083 Huang, Y., Lu, R., Chen, K., 2017. Development of a multichannel hyperspectral imaging probe
1084 for property and quality assessment of horticultural products. *Postharvest Biol. Technol.* 133,
1085 88-97.

1086 Huang, Y., Lu, R., Chen, K., 2018a. Prediction of firmness parameters of tomatoes by portable
1087 visible and near-infrared spectroscopy. *J. Food Eng.* 222, 185-198.

1088 Huang, Y., Lu, R., Chen, K., 2018b. Quality assessment of tomato fruit by optical absorption and
1089 scattering properties. *Postharvest Biol. Technol.* 143, 78-85.

1090 Huang, Y., Lu, R., Chen, K., 2018c. Prediction of tomato firmness using spatially-resolved
1091 spectroscopy. *Postharvest Biol. Technol.* 140, 18-26.

1092 Jacquez, J.A., Kuppenheim, H.F., 1955. Theory of the integrating sphere. *J. Opt. Soc. America.*
1093 55, 460-470.

1094 Kienle, A., Patterson, M.S., 1997. Improved solutions of the steady-state and the time-resolved
1095 diffusion equations for reflectance from a semi-infinite turbid medium. *J. Opt. Soc. America*
1096 *A* 14, 246-254.

1097 Lancaster, J.E., Grant, J.E., Lister, C.E., Taylor, M.C., 1994. Skin color in apples - Influence of
1098 copigmentation and plastid pigments on shade and darkness of red color in five genotypes. *J.*
1099 *Am. Soc. Hort. Sci.* 119, 63–69.

1100 Langerholc, J., 1982. Beam broadening in dense scattering media. *Appl. Opt.* 21, 1593-1598.

1101 Leyre, S., Durinck, G., Van Giel, B., Saeys, W., Hofkens, J., Deconinck, G., Hanselaer, P., 2012.
1102 Extended adding-doubling method for fluorescent applications. *Opt. Express* 20, 17856–
1103 17872.

1104 Li, R., Lu, Y., Lu, R., 2018. Structured illumination reflectance imaging for detection of
1105 subsurface tissue bruising in apples. *Trans. ASABE* 61, 809-819.

1106 López-Maestresalas, A., Aernouts, B., Van Beers, R., Arazuri, S., Jarén, C., de Baerdemaeker, J.,
1107 Saeys, W., 2015. Bulk optical properties of potato flesh in the 500–1900 nm range. *Food*
1108 *Bioprocess Technol.* 9, 463–470.

1109 Lorente, D., Aleixos, N., Gómez-Sanchis, J., Cubero, S., Blasco, J., 2013. Selection of optimal
1110 wavelength features for decay detection in citrus fruit using the ROC curve and neural
1111 networks. *Food Bioprocess Technol.* 6, 530-541.

1112 Lorente, D., Zude, M., Idler, C., Gómez-Sanchis, J., Blasco, J., 2015. Laser-light backscattering
1113 imaging for early decay detection in citrus fruit using both a statistical and a physical model.
1114 *J. Food Eng.* 154, 76–85.

1115 Lu, R., 2004. Multispectral imaging for predicting firmness and soluble solids content of apple
1116 fruit. *Postharvest Biol. Technol.* 31, 147-157.

1117 Lu, R., 2008. Quality evaluation of fruit by hyperspectral imaging. In: Sun, D.W. (Eds.),
1118 *Computer Vision Technology for Food Quality Evaluation.* Academic Press, Cambridge,
1119 MA, USA, pp. 319–348.

1120 Lu, R. (Ed.), 2016. *Light Scattering Technology for Food Property, Quality and Safety*
1121 *Assessment.* CRC Press, Boca Raton, FL, USA.

1122 Lu, R., Ariana, D.P., Cen, H., 2011. Optical absorption and scattering properties of normal and
1123 defective picking cucumber for 700-1000 nm. *Sens. & Instrumen. Food Qual.* 5, 51-56.

1124 Lu, R., Cen, H., Huang, M., Ariana, D.P., 2010. Spectral absorption and scattering properties of
1125 normal and bruised apple tissue. *Trans. ASABE* 53, 263-269.

1126 Lu, Y., 2018. Development of Structred Illumination Reflectance Imaging Technique as a New
1127 Modality for Enhanced Defect Detection of Apples. Ph.D. dissertation, Michigan State
1128 University, East Lansing, MI, USA, 253pp.

1129 Lu, Y., Huang, Y., Lu, R., 2017. Innovative hyperspectral imaging-based techniques for quality
1130 evaluation of fruits and vegetables: A review. *Appl. Sci.* 7, 189.

- 1131 Lu, Y., Li, R., Lu, R., 2016a. Structured-illumination reflectance imaging (SIRI) for enhanced
1132 detection of fresh bruises in apples. *Postharvest Biol. Technol.* 117, 89-93.
- 1133 Lu, Y., Li, R., Lu, R., 2016b. Fast demodulation of pattern images by spiral phase transform in
1134 structured-illumination reflectance imaging for detection of bruises in apples. *Comp. Elec.*
1135 *Agric.* 127, 652-658.
- 1136 Lu, Y., Li, R., Lu, R., 2016c. Gram-Schmidt orthonormalization for retrieval of amplitude
1137 images under sinusoidal patterns of illumination. *Appl. Opt.* 55, 6866-6873.
- 1138 Lu, Y., Lu, R., 2017a. Non-destructive defect detection of apples by spectroscopic and imaging
1139 technologies: A review. *Trans. ASABE* 60, 1765-1790.
- 1140 Lu, Y., Lu, R. 2017b. Development of a multispectral structured-illumination reflectance
1141 imaging (SIRI) system and its applications to bruise detection of apples. *Trans. ASABE* 60,
1142 1379-1389.
- 1143 Lurie, S., Vanoli, M., Daga, A., Weksler, A., Lovati, F., Eccher Zerbini, P., Spinelli, L.,
1144 Torricelli, A., Feng, J., Rizzolo, A., 2011. Chilling injury in stored nectarines and its
1145 detection by time-resolved reflectance spectroscopy. *Postharvest Biol. Technol.* 59, 211-218.
- 1146 Malsan, J., Gurjar, R., Wolf, D., Vishwanath, K., 2014. Extracting optical properties of turbid
1147 media using radially and spectrally resolved diffuse reflectance. *Proc. SPIE.* 8936, 893615,
1148 SPIE, Bellingham, WA, USA.
- 1149 Marquet, P., Bevilacqua, F., Depeursinge, C., Dehaller, E.B., 1995. Determination of reduced
1150 scattering and absorption-coefficients by a single charge-coupled-device array measurement.
1151 I. comparison between experiments and simulations. *Opt. Eng.* 34, 2055-2063.
- 1152 Martelli, F., Del Bianco, S., Ismaelli, A., Zaccanti, G., 2010. *Light Propagation through
1153 Biological Tissue and Other Diffusive Media.* SPIE Press, Bellingham, WA, USA.
- 1154 Merzlyak, M.N., Solovchenko, A.E., Gitelson, A.A., 2003. Reflectance spectral features and
1155 non-destructive estimation of chlorophyll, carotenoid and anthocyanin content in apple fruit.
1156 *Postharvest Biol. Technol.* 27, 197-211.
- 1157 Mollazade, K., Arefi, A., 2017. Optical analysis using monochromatic imaging-based spatially-
1158 resolved technique capable of detecting mealiness in apple fruit. *Sci. Hortic.* 225, 589-598.
- 1159 Mollazade, K., Omid, M., Tab, F.A., Kalaj, Y.R., Mohtasebi, S.S., Zude, M., 2013. Analysis of
1160 texture-based features for predicting mechanical properties of horticultural products by laser
1161 light backscattering imaging. *Comp. Electr. Agric.* 98, 34-45.
- 1162 Nguyen Do Trong, N., Erikinbaev, C., Tsuta, M., De Baerdemaeker, J., Nicolai, B.M., Saeys,
1163 W., 2014a. Spatially resolved diffuse reflectance in the visible and near-infrared wavelength
1164 range for non-destructive quality assessment of 'Braeburn' apples. *Postharvest Biol. Technol.*
1165 91, 39-48.
- 1166 Nguyen Do Trong, N., Rizzolo, A., Herremans, E., Vanoli, M., Cortellino, G., Erkinbaev, C.,
1167 Tsuta, M., 2014b. Optical properties-microstructure-texture relationships of dried apple
1168 slices: Spatially resolved diffuse reflectance spectroscopy as a novel technique for analysis
1169 and process control. *Innovative Food Sci. Emerg. Technol.* 21, 160-168.
- 1170 Nicolai, B.M., Beullens, K., Bobelyn, E., Peirs, A., Saeys, W., Theron, K.I., Lammertyn, J.,
1171 2007. Nondestructive measurement of fruit and vegetable quality by means of NIR
1172 spectroscopy: A review. *Postharvest Biol. Technol.* 46, 99-118.
- 1173 Nicolai, B.M., Verlinden, B.E., Desmet, M., Saevels, S., Saeys, W., Theron, K., Cubeddu, R.,
1174 Pifferi, A., Torricelli, A., 2008. Time-resolved and continuous wave NIR reflectance
1175 spectroscopy to predict soluble solids content and firmness of pear. *Postharvest Biol.*
1176 *Technol.* 47, 68-74.

1177 Patterson, M.S., Chance, B., Wilson, B.C., 1989. Time resolved reflectance and transmittance for
1178 the non-invasive measurement of tissue optical properties. *Appl. Opt.* 28, 2331-2336.

1179 Patterson, M.S., Moulton, J.D., Wilson, B.C., Berndt, K.W., Lakowicz, J.R. 1991. Frequency-
1180 domain reflectance for the determination of the scattering and absorption properties of tissue.
1181 *Appl. Opt.* 30, 4474-4476.

1182 Peng, Y., Lu, R., 2005. Modeling multispectral scattering profiles for prediction of apple fruit
1183 firmness. *Trans. ASABE* 48, 235-242.

1184 Peng, Y., Lu, R., 2006. Improving apple fruit firmness predictions by effective correction of
1185 multispectral scattering images. *Postharvest Biol. Technol.* 41, 266-274.

1186 Peng, Y., Lu, R., 2007. Prediction of apple fruit firmness and soluble solids content using
1187 characteristics of multispectral scattering imaging. *J. Food Eng.* 82, 142-152.

1188 Peng, Y., Lu, R., 2008. Analysis of spatially resolved hyperspectral scattering images for
1189 assessing apple fruit firmness and soluble solids content. *Postharvest Biol. Technol.* 48(1),
1190 52-62.

1191 Pereira, T., Tijskens, L.M.M., Vanoli, M., Rizzolo, A., Eccher Zerbini, P., Torricelli, A.,
1192 Spinelli, L., Filgueiras, H., 2010. Assessing the harvest maturity of Brazilian mangoes. *Acta*
1193 *Hortic.* 880, 269-276.

1194 Pickering, J.W., Prah, S.A., van Wieringen, N., Beek, J.F., Sterenborg, H.J.C.M., van Gemert,
1195 M.J.C., 1993. Double-integrating-sphere system for measuring the optical properties of
1196 tissue. *Appl. Opt.* 32, 399-410.

1197 Pifferi, A., Taroni, P., Torricelli, A., Messina, F., Cubeddu, R., 2003. Four-wavelength time-
1198 resolved optical mammography in the 680–980 nm range. *Opt. Lett.* 28 1138–40.

1199 Pilz, M., Honold, S., Kienle, A., 2008. Determination of the optical properties of turbid media by
1200 measurements of the spatially resolved reflectance considering the point-spread function of
1201 the camera system. *J. Biomed. Opt.* 13, 054047.

1202 Pogue, B.W., Patterson, M.S., 2006. Review of tissue simulating phantoms for optical
1203 spectroscopy, imaging and dosimetry. *J. Biomed. Opt.* 11, 041102.

1204 Postelmans, A., Aernouts, B., Sayes, W., 2018. Estimation of partical size distributions from
1205 bulk scattering spectra: sensitivitiy to distribution type and spectral noise. *Opt. Express* 26,
1206 15015-15038.

1207 Prah, S.A., 2011. Everything I Think You Should Know About Inverse Adding-Doubling.
1208 <https://omlc.org/software/iad/manual.pdf>.

1209 Prah, S.A., 1995. The adding doubling method. In: Welch, A.J., van Gemert, M.J.C. (Eds.),
1210 *Optical-Thermal Response of Laser Irradiated Tissue*, Springer, New York, NY, USA, pp.
1211 101-129.

1212 Prah, S.A., van Gemert, M. J.C., Welch, A.J., 1993. Determining the optical properties of turbid
1213 media by using the adding-doubling method. *Appl. Opt.* 32, 559–568.

1214 Qin, J., Lu, R., 2007. Measurement of the absorption and scattering properties of turbid liquid
1215 foods using hyperspectral imaging. *Appl. Spectr.* 61, 388-396.

1216 Qin, J., Lu, R., 2008. Measurement of the optical properties of fruits and vegetables using
1217 spatially resolved hyperspectral diffuse reflectance imaging technique. *Postharvest Biol.*
1218 *Technol.* 49, 355–365.

1219 Qin, J., Lu, R., 2009. Monte Carlo simulation for quantification of light transport features in
1220 apples. *Comput. Electron Agric.* 68, 44-51.

1221 Qin, J., Lu, R., Peng, Y., 2009. Prediction of apple internal quality using spectral absorption and
1222 scattering properties. *Trans. ASABE* 52, 499-507.

- 1223 Qing, Z., Ji, B., Zude, M., 2008. Non-destructive analyses of apple quality parameters by means
1224 of laser-induced light backscattering imaging. *Postharvest Biol. Technol.* 48, 215-222.
- 1225 Reynolds, L., Johnson, C., Ishimaru, A., 1976. Diffuse reflectance from a finite blood medium-
1226 applications to modeling of fiber optic catheters. *Appl. Optics* 15, 2059-2067.
- 1227 Rizzolo, A., Bianchi, G., Vanoli, M., Lurie, S., Spinelli, L., Torricelli, A., 2013. Electronic nose
1228 to detect volatile compound profile and quality changes in ‘Spring Belle’ peach (*Prunus*
1229 *persica* L.) during cold storage in relation to fruit optical properties measured by time-
1230 resolved reflectance spectroscopy. *J. Agric. Food Chem.*, 61, 1671-1685.
- 1231 Rizzolo, A., Vanoli, M., 2016. Time-resolved technique for measuring optical properties and
1232 quality of food. In: Lu, R. (Ed.), *Light Scattering Technology for Food Property, Quality and*
1233 *Safety Assessment*. CRC Press, Boca Raton, FL, pp. 187-224
- 1234 Rizzolo, A., Vanoli, P., Bianchi, G., 2014a. Relationship between texture sensory profiles and
1235 optical properties measured by time-resolved reflectance spectroscopy during post storage
1236 shelf life of ‘Braeburn’ apples. *J. Hort. Res.* 22, 113-121.
- 1237 Rizzolo, A., Vanoli, M., Cortellino, G., Spinelli, L., Contini, D., Herremans, E., Bongaers, E.,
1238 Nemeth, A., Leitner, M., Verboven, P., Nicolai, B.M., Torricelli, A., 2014b. Characterizing
1239 the tissue of apple air-dried and osmo-air-dried rings by X-CT and OCT and relationship
1240 with ring crispness and fruit maturity at harvest measured by TRS. *Innovative Food Sci.*
1241 *Emerg. Technol.* 24, 121-130.
- 1242 Rizzolo, A., Vanoli, M., Cortellino, G., Spinelli, L., Torricelli, A., 2011. Quality characteristics
1243 of air dried apple rings: Influence of storage time and fruit maturity measured by time-
1244 resolved reflectance spectroscopy. *Porcedia Food Sci.*, 1, 216-223.
- 1245 Rizzolo, A., Vanoli, M., Eccher Zerbini, P., Spinelli, L., Torricelli, A., 2010a. Influence of cold
1246 storage time on the softening prediction in ‘Spring Bright’ nectarines. *Acta Hort.* 877,
1247 1395-1402.
- 1248 Rizzolo, A., Vanoli, M., Spinelli, L., Torricelli, A., 2010b. Sensory characteristics, quality and
1249 optical properties measured by time-resolved reflectance spectroscopy in stored apples.
1250 *Postharvest Biol. Technol.* 58, 1-12.
- 1251 Romano, G., Nagle, M., Argyropoulos, D., Muller, J., 2011. Laser light backscattering to
1252 monitor moisture content, soluble solid content and hardness of apple tissues during drying.
1253 *J. Food Eng.* 104, 657-662.
- 1254 Rowe, P.I., Künemeyer, R., McGlone, A., Talele, S., Martinsen, P., Seelye, R., 2014.
1255 Relationship between tissue firmness and optical properties of ‘Royal Gala’ apples from 400
1256 to 1050 nm. *Postharvest Biol. Technol.* 94, 89-96.
- 1257 Saeys, W., Velazco-Roa, M.A., Thennadil, S.N., Ramon, H., Nicolai, B.M., 2008. Optical
1258 properties of apple skin and flesh in the wavelength range from 350 to 2200 nm. *Appl. Opt.*
1259 47, 908-919.
- 1260 Seifert, R., Zude, M., Spinelli, L., Torricelli, A., 2015. Optical properties of developing pip and
1261 stone fruit reveal underlying structural changes. *Physiol. Plant.* 153, 327-336.
- 1262 Sharma, M., Hennessy, R., Markey, M.K., Tunnell, J.W., 2014. Verification of a two-layer
1263 inverse Monte Carlo absorption model using multiple source-detector separation diffuse
1264 reflectance spectroscopy. *Biomed. Opt. Express* 5, 40.
- 1265 Simpson, T.W., Poplinski, J.D., Koch, P.N., Allen, J.K., 2001. Metamodels for computer-based
1266 engineering design: Survey and recommendations. *Eng. Comput.* 17, 129-150.
- 1267 Spinelli, L., Rizzolo, A., Vanoli, M., Grassi, M., Eccher Zerbini, P., de Azevedo Pimentel, R.M.,
1268 Torricelli, A., 2012. Optical properties of pulp and skin in Brazilian mangoes in the 540-900

1269 nm spectral region: implication for non-destructive maturity assessment by time-resolved
1270 reflectance spectroscopy. Proceedings of the 3rd CIGR International Conference of
1271 Agricultural Engineering (CIGR-AgEng2012), July 8-12, Valencia, Spain.

1272 Sun, J., Kunnemeyer, R., McGlone, A., Rowe, P., 2017. Multispectral scattering imaging and
1273 NIR interactance for apple firmness predictions. *Postharvest Biol. Technol.* 119, 58-68.

1274 Sun, Y., Lu, R., Lu, Y., Tu, K., Pan, L., 2019. Detection of early decay in peaches by structured-
1275 illumination reflectance imaging. *Postharvest Bio. Technol.* (in press)

1276 Tijskens, L.M.M., Eccher Zerbini, P., Schouten, R.E., 2007a. Biological variation in ripening of
1277 nectarine. *Veg. Crops Res. Bull.* 66, 205-212.

1278 Tijskens, L.M.M., Eccher Zerbini, P., Schouten, R.E., Vanoli, M., Jacob, S., Grassi, M.,
1279 Cubeddu, R., Spinelli, L., Torricelli, A., 2007b. Assessing harvest maturity in nectarines.
1280 *Postharvest Biol. Technol.* 45, 204-213.

1281 Torricelli, A., 2009. Determination of optical properties in turbid media: time-resolved approach.
1282 In: Zude, M. (Ed.). *Optical Monitoring of Fresh and Processed Agricultural Crops*. CRS
1283 Press, Boca Raton, FL, USA, pp. 55-81.

1284 Tu, K., Jancsok, P., Nicolai, B., De Baerdemaeker, J., 2000. Use of laser-scattering imaging to
1285 study tomato-fruit quality in relation to acoustic and compression measurements. *Int. J. Food*
1286 *Sci. Technol.* 35, 503–510.

1287 Tuchin, V.V., 2007. *Tissue Optics: Light Scattering Methods and Instruments for Medical*
1288 *Diagnosis*. SPIE Press, Bellingham, WA, USA.

1289 Valero, C., Barreiro, P., Ruiz-Altisent, M., Cubeddu, R., Pifferi, A., Taroni, P., Torricelli, A.,
1290 2005. Mealiness detection in apples using time resolved reflectance spectroscopy. *J. Texture*
1291 *Stud.* 36, 439-458.

1292 Valero, C., Ruiz-Altisent, M., Cubeddu, R., Pifferi, A., Taroni, P., Torricelli, A., Valentini, G.,
1293 Johnson, D.S., Dover, C. J., 2004. Detection of internal quality in kiwi with time-domain
1294 diffuse reflectance spectroscopy. *Appl. Eng. Agric.* 20, 223-230.

1295 Van Beers, R., Aernouts, B., León Gutiérrez, L., Erkinbaev, C., Rutten, K., Schenk, A., Nicolai,
1296 B., Saeys, W., 2015. Optimal illumination-detection distance and detector size for predicting
1297 Braeburn apple maturity from Vis/NIR laser reflectance measurements. *Food Bioprocess*
1298 *Technol.* 8, 2123–2136.

1299 Van Beers, R., Aernouts, B., Reis, M.M., Saeys, W., 2017a. Anisotropic light propagation in
1300 bovine muscle tissue depends on the initial fiber orientation, muscle type and wavelength.
1301 *Opt. Express* 25, 22082-22095.

1302 Van Beers, R., Aernouts, B., Watté, R., Schenk, A., Nicolai, B., Saeys, W., 2017b. Effect of
1303 maturation on the bulk optical properties of apple skin and cortex in the 500–1850 nm
1304 wavelength range. *J. Food Eng.* 214, 79-89.

1305 Van Beers, R., Kokawa, M., Aernouts, B., Watté, R., De Smet, S., Saeys, W., 2018. Evolution of
1306 the bulk optical properties of bovine muscles during wet aging. *Meat Sci.* 136, 50-58.

1307 van de Hulst, H.C., 1980. *Multiple Light Scattering: Tables, Formulas, and Applications*.
1308 Academic Press, New York.

1309 Vangdal, E., Vanoli, M., Rizzolo, A., Eccher Zerbini, P., Spinelli, L., Torricelli, A., 2012.
1310 Detecting internal physiological disorders in stored plums (*Prunus domestica* L.) by time-
1311 resolved reflectance spectroscopy. *Acta Hort.* 945, 197-203.

1312 Vanoli, M., Rizzolo, A., Eccher Zerbini, P., Spinelli, L., Torricelli, A., 2009. Nondestructive
1313 detection of internal defects in apple fruit by time-resolved reflectance spectroscopy. In:

1314 Nuenes, C. (Ed.), *Environmentally Friendly and Safe Technologies for Quality of Fruits and*
1315 *Vegetables*. 20-26, Universidade do Algarve, Portugal.

1316 Vanoli, M., Rizzolo, A., Grassi, M., Farina, A., Pifferi, A., Spinelli, L., Torricelli, A., 2011.
1317 Time-resolved reflectance spectroscopy nondestructively reveals structural changes in ‘Pink
1318 Lady®’ apples during storage. *Procedia Food Sci.* 1, 81-89.

1319 Vanoli, M., Rizzolo, A., Grassi, M., Spinelli, L., Zanella, A., Torricelli, A., Zanella, A., Spinelli,
1320 L., 2015. Characterizing apple texture during storage through mechanical, sensory and optical
1321 properties. *Acta Hort.* 11078, 383-390.

1322 Wang, A., Lu, R., Xie, L., 2017a. A sequential method for measuring the optical properties of
1323 two-layer media with spatially-resolved reflectance: simulation study. In: Kim, M., Chao, K.,
1324 Chin, B.A., (Eds.), *Sensing for Agriculture and Food Quality and Safety VIII*, SPIE
1325 Proceedings 9864, 98640Q, 12pp. SPIE (The International Society for Optical Engineering),
1326 Bellingham, WA.

1327 Wang, A., Lu, R., Xie, L., 2017b. Improved algorithm for estimating the optical properties of
1328 food products using spatially-resolved diffuse reflectance. *J. Food Eng.* 212, 1-11.

1329 Wang, L., Jacques, S.L., Zheng, L., 1995. MCML- Monte Carlo modeling of light transport in
1330 multi-layered tissues. *Comput. Methods Programs Biomed.* 47, 131–46.

1331 Wang, L.V., Jacques, S.L., 2000. Source of error in calculation of optical diffuse reflectance
1332 from turbid media using diffusion theory. *Comput. Methods Programs Biomed.* 61, 163–70.

1333 Wang, W., Li, C., 2013. Measurement of the light absorption and scattering properties of onion
1334 skin and flesh at 633 nm. *Postharvest Biol. Technol.* 86, 494-501.

1335 Wang, W., Li, C., Gitaitis, R.D., 2014. Optical properties of healthy and diseased onion tissues in
1336 the visible and near-infrared spectral region. *Trans. ASABE* 57, 1771-1782.

1337 Wang, L.V., Wu, H.I., 2007. *Biomedical Optics: Principles and Imaging*. John Wiley & Sons,
1338 Hoboken, NJ, USA.

1339 Watté, R., Aernouts, B., Saeys, W., 2016. Monte Carlo modeling of light transfer in food. In: Lu,
1340 R. (Ed.), *Light Scattering Technology for Food Property, Quality and Safety Assessment*
1341 CRC Press, Boca Raton, FL, USA, pp 79–109. doi:10.1201/b20220-5

1342 Watté, R., Aernouts, B., Van Beers, R., Herremans E., Ho, Q.T., Verboven, P., Nicolai,
1343 B., Saeys, W., 2015a. Modeling the propagation of light in realistic tissue structures with
1344 MMC-fpf: a meshed Monte Carlo method with free phase function. *Opt. Express* 23, 17467-
1345 17486.

1346 Watté, R., Aernouts, B., Van Beers, R., Saeys, W., 2015b. Robust metamodel-based inverse
1347 estimation of bulk optical properties of turbid media from spatially resolved diffuse
1348 reflectance measurements. *Opt. Express* 5, 27880–27898.

1349 Watté, R., Nguyen Do Trong, N., Aernouts, B., Erkinbaev, C., De Baerdemaeker, J., Nicolai, B.,
1350 Saeys, W., 2013. Metamodeling approach for efficient estimation of optical properties of
1351 turbid media from spatially resolved diffuse reflectance measurements. *Opt. Express* 21,
1352 32630-32642.

1353 Xia, J.J., Berg, E.P., Lee, J.W., Yao, G., 2007. Characterizing beef muscles with optical
1354 scattering and absorption coefficients in VIS-NIR region. *Meat Sci.* 75, 78-83.

1355 Xia, J.J., Weaver, A., Gerrard, D.E., Yao, G., 2008. Distribution of optical scattering properties
1356 in four beef muscles. *Sens. Instr. Food Qual. Safety* 2, 75-81.

1357 Zamora-Rojas, E., Aernouts, B., Garrido-Varo, A., Pérez-Marín, D., Guerrero-Ginel, J. E.,
1358 Saeys, W., 2013. Double integrating sphere measurements for estimating optical properties
1359 of pig subcutaneous adipose tissue. *Innovative Food Sci. Emerg. Technol.*, 19, 218–226.

- 1360 Zhang, M., Li, C., Fan, S., 2017a. Optical properties of healthy and bruised blueberry tissue in
1361 the near-infrared spectral region. ASABE Paper #1700423. ASABE, St. Joseph, MI, USA.
- 1362 Zhang, M., Li, C., Yang, F., 2019. Optical properties of blueberry flesh and skin and Monte
1363 Carlo multi-layered simulation of light interaction with fruit tissues. *Postharvest Biol.*
1364 *Technol.* 150, 28-41.
- 1365 Zhang, S., Wu, X., Zhang, S., Cheng, Q., Tan, Z., 2017b. An effective method to inspect and
1366 classify the bruising degree of apples based on the optical properties. *Postharvest Biol.*
1367 *Technol.* 127, 44-52.
- 1368 Zhu, Q., He, C., Lu, R., Mendoza, F., Cen, H., 2015. Ripeness evaluation of 'Sun Bright' tomato
1369 using optical absorption and scattering properties. *Postharvest Biol. Technol.* 103, 27-34.